

AFAL-TR-77-112



AD A047311

APPLICATION OF THE PLANE WAVE EXPANSION METHOD TO PERIODIC ARRAYS HAVING A SKEWED GRID GEOMETRY

The Ohio State University
ElectroScience Laboratory
Department of Electrical Engineering
Columbus, Ohio 43212

October 1977

TECHNICAL REPORT AFAL-TR-77-112

Approved for public release; distribution unlimited.

AD No. _____

FILE COPY

AIR FORCE AVIONICS LABORATORY
AIR FORCE WRIGHT AERONAUTICAL LABORATORIES
AIR FORCE SYSTEMS COMMAND
WRIGHT-PATTERSON AIR FORCE BASE, OHIO 45433

DDC
RECEIVED
DEC 6 1977
D

NOTICE

When Government drawings, specifications, or other data are used for any purpose other than in connection with a definitely related Government procurement operation, the United States Government thereby incurs no responsibility nor any obligation whatsoever; and the fact that the government may have formulated, furnished, or in any way supplied the said drawings, specifications, or other data, is not to be regarded by implication or otherwise as in any manner licensing the holder or any other person or corporation, or conveying any rights or permission to manufacture, use, or sell any patented invention that may in any way be related thereto.

This report has been reviewed by the Information Office (OI) and is releasable to the National Technical Information Service (NTIS). At NTIS, it will be available to the general public, including foreign nations.

This technical report has been reviewed and is approved for publication.

Larry E. Carter

Larry E. Carter
Project Engineer

William F. Bahret

William F. Bahret
Chief, Passive ECM Branch
Electronic Warfare Division

FOR THE COMMANDER

Joseph H. Jacobs

JOSEPH H. JACOBS, Colonel, USAF
Chief, Electronic Warfare Division

Copies of this report should not be returned unless return is required by security consideration, contractual obligations, or notice on a specific document.

19 REPORT DOCUMENTATION PAGE		READ INSTRUCTIONS BEFORE COMPLETING FORM	
1. REPORT NUMBER 18 AFAL TR-77-112	2. GOVT ACCESSION NO.	3. RECIPIENT'S CATALOG NUMBER 9	
3. TITLE (and Subtitle) 6 APPLICATION OF THE PLANE WAVE EXPANSION METHOD TO PERIODIC ARRAYS HAVING A SKEWED GRID GEOMETRY.		4. TYPE OF REPORT & PERIOD COVERED Technical Report.	
7. AUTHOR(S) 10 T. W./Kornbau		5. PERFORMING ORG. REPORT NUMBER 14 ESL-4346-3	8. CONTRACT OR GRANT NUMBER(S) Contract F33615-76-C-1024 15
9. PERFORMING ORGANIZATION NAME AND ADDRESS The Ohio State University ElectroScience Laboratory, Department of Electrical Engineering Columbus, Ohio 43212		10. PROGRAM ELEMENT, PROJECT, TASK AREA & WORK UNIT NUMBERS 16 Project 76331328 62264 F 17 13	
11. CONTROLLING OFFICE NAME AND ADDRESS Air Force Avionics Laboratory (AFAL/WRP) Air Force Wright Aeronautical Laboratories Wright-Patterson Air Force Base, Ohio 45433		12. REPORT DATE 11 Oct 1977	13. NUMBER OF PAGES 12 71 p.
14. MONITORING AGENCY NAME & ADDRESS (if different from Controlling Office)		15. SECURITY CLASS. (of this report) Unclassified	
15a. DECLASSIFICATION/DOWNGRADING SCHEDULE			
16. DISTRIBUTION STATEMENT (of this Report) Approved for public release; distribution unlimited			
17. DISTRIBUTION STATEMENT (of the abstract entered in Block 20, if different from Report)			
18. SUPPLEMENTARY NOTES			
19. KEY WORDS (Continue on reverse side if necessary and identify by block number) Metallic radome Mutual admittance Skewed grid Plane wave expansion Generalized three legged element			
20. ABSTRACT (Continue on reverse side if necessary and identify by block number) This report extends the Plane Wave Expansion Method of calculating the performance of periodic arrays to include arrays with a skewed grid structure. Previously, only rectangular grids could be calculated using this method. The Plane Wave Expansion Method is important since it may be used to calculate performance of arrays imbedded in dielectric and arrays with almost any element geometry. → next page			

20.

→ This work is important to the Air Force in that it enables us to compute metallic radome surfaces where the elements are located in a skewed fashion. This is a crucial step in designing metallic radomes of arbitrary shape.

This added dimension to the Plane Wave Expansion Method has been used to investigate arrays of generalized three legged elements in a triangular grid structure.

ACCESSION FOR		
ATIS	White Section	<input checked="" type="checkbox"/>
DDC	Post Section	<input type="checkbox"/>
CHANGES		<input type="checkbox"/>
JUSTIFICATION		
BY		
DISTRIBUTION/AVAILABILITY CODES		
Dist.	AVA L. EDC	SPECIAL
A		

DDC
 RECEIVED
 DEC 6 1977
 RECEIVED
 D

FOREWORD

This report, Ohio State University Research Foundation Report No. 4346-3, was prepared by the ElectroScience Laboratory, Department of Electrical Engineering, The Ohio State University at Columbus, Ohio. Research was conducted under Contract F33615-76-C-1024 of the Air Force Avionics Laboratory at Wright-Patterson Air Force Base, Ohio. Mr. L. E. Carter, AFAL-WRP was the AFAL Program Monitor for this research conducted under Project No. 7633.

The material contained in this report is also used as a thesis submitted to the Department of Electrical Engineering, The Ohio State University as partial fulfillment for the degree Master of Science.

The author wishes to express his gratitude to the individuals at the ElectroScience Laboratory who assisted in work involved in this thesis. A special thanks goes to Dr. Benedikt Munk for his counsel in all phases of the investigation. The help of Dr. Edward Pelton in the early stages of the investigation is also appreciated.

CONTENTS

Section	Page
I INTRODUCTION.....	1
II DERIVATION.....	4
III APPLICATION OF RESULTS.....	13
A. Straight Dipole Arrays	13
B. Slot Arrays of Generalized Three Legged Elements	15
1. Background	15
2. Optimum Grid-Element Combinations	25
3. Analysis of Results	34
IV CONCLUSIONS.....	53
APPENDIX A - GRATING LOBES IN ARRAYS HAVING A SKEWED GRID.....	54
APPENDIX B - ARRAY GRID ANGLE RELATIONSHIPS.....	56
APPENDIX C - SAMPLE CALCULATIONS OF ADMITTANCE RELATIONSHIPS...	58
REFERENCES.....	61

LIST OF FIGURES

Figure		Page
1	An array of straight dipoles having a rectangular grid structure.	2
2	An array of straight dipoles having a skewed grid structure.	3
3	A view of the arbitrary grid structure to be considered, showing the parameters D_x , D_z and Δz .	5
4	The input impedance of an element in an array of z oriented dipoles having various amounts of skew. The angle of incidence, ζ is measured from the normal.	14
5	Reflection coefficient versus frequency for an array of z oriented dipoles in a rectangular grid.	16
6	Reflection coefficient versus frequency for an array of z oriented dipoles having a grid structure such that $\Delta z = .5 D_z$.	17
7	Generalized three legged element showing critical parameters.	18
8	The voltage modes induced on a generalized three legged element.	20
9	Portion of an equilateral triangular grid array with 120° between the element legs. Also, the angle which defines the plane of incidence.	23
10	Magnitudes of the transmitted field (left scale) and cross component (right scale) versus frequency for a slot array having an equilateral triangular grid and 120° between the element legs. The symbols (\parallel/\perp) denote the H-field (parallel/perpendicular) to the plane of incidence defined by α .	24
11	Grid structure depicting the variables involved with the investigation: top grid angle (TGA), side grid angle (SGA), leg angle (LA), and D_x , D_z and Δz , the array parameters.	26
12	Magnitudes of the transmitted field (left scale) and cross component (right scale) versus frequency for the 55/120 (TGA/LA) slot array. The symbols (\parallel/\perp) denote the H-field (parallel/perpendicular) to the plane of incidence defined by α .	27

13	Magnitudes of the transmitted field (left scale) and cross component (right scale) versus frequency for the 55/110 (TGA/LA) slot array. The symbols (\parallel/\perp) denote the H-field (parallel/perpendicular) to the plane of incidence defined by α .	28
14	Magnitudes of the transmitted field (left scale) and cross component (right scale) versus frequency for the 55/105 (TGA/LA) slot array. The symbols (\parallel/\perp) denote the H-field (parallel/perpendicular) to the plane of incidence defined by α .	29
15	Magnitudes of the transmitted field (left scale) and cross component (right scale) versus frequency for the 65/120 (TGA/LA) slot array. The symbols (\parallel/\perp) denote the H-field (parallel/perpendicular) to the plane of incidence defined by α .	32
16	Magnitudes of the transmitted field (left scale) and cross component (right scale) versus frequency for the 65/135 (TGA/LA) slot array. The symbols (\parallel/\perp) denote the H-field (parallel/perpendicular) to the plane of incidence defined by α .	33
17	Perpendicular component of the pattern factor of the symmetric voltage mode for leg angles of 105° and 135° .	35
18	Perpendicular component of the pattern factor of the asymmetric voltage mode for leg angles of 105° and 135° .	36
19	Parallel component of the pattern factor of the symmetric voltage mode for leg angles of 105° and 135° .	37
20	Parallel component of the pattern factor of the asymmetric voltage mode for leg angles of 105° and 135° .	38
21	Magnitude of the admittance Y_{ss}^{rest} for various incidence directions at a frequency slightly below resonance. Depicted are the 60/120, 55/120, and 65/120 arrays. (The phase is -90°).	39
22	Magnitude of the admittance Y_{aa}^{rest} for various incidence directions at a frequency slightly below resonance. Depicted are the 60/120, 55/120 and 65/120 arrays. (The phase is -90°).	40

23	Magnitude (left scale) and phase (right scale) of the admittance Y_{as}^{rest} for the 60/120 array. Frequency is slightly below resonance.	41
24	Magnitude (left scale) and phase (right scale) of the admittance Y_{as}^{rest} for the 55/120 array. Frequency is slightly below resonance.	46
25	Polar plot of the admittance Y_{as}^{rest} for incidence angles of 30° for 65/120, 60/120, and 55/120 arrays. Frequency is slightly below resonance.	47
26	Magnitude (left scale) and phase (right scale) of the admittance. Y_{as}^{rest} for the 65/120 array. Frequency is slightly below resonance.	48
27	Magnitude (left scale) and phase (right scale) of the admittance Y_{as}^{rest} for the 60/105 array. Frequency is slightly below resonance.	49
28	Magnitude (left scale) and phase (right scale) of the admittance Y_{as}^{rest} for the 55/105 array. Frequency is slightly below resonance.	50
29	Magnitude (left scale) and phase (right scale) of the admittance Y_{as}^{rest} for the 60/135 array. Frequency is slightly below resonance.	51
30	Magnitude (left scale) and phase (right scale) of the admittance Y_{as}^{rest} for the 65/135 arrays. Frequency is slightly below resonance.	52
B1	General skewed grid structure showing the relationship between the top and side grid angles.	57

SECTION I INTRODUCTION

Periodic surfaces are being investigated for use in an ever widening range of applications such as metallic radomes and reflectors. To obtain the desired electrical performance of a metallic radome, for example, it has been found that complicated surfaces are needed [1]. It is important to be able to calculate the performance of these complex surfaces. The two variables involved in a periodic array are element geometry and grid structure (the location of the elements with respect to one another). In the metallic radome application, the grid structure must be modified in order to construct the surface into the shape of the radome. This grid modification makes a modification in the element geometry necessary in order to maintain the desired electrical performance.

Pelton addressed this problem by investigating the effect of altering both element shape and grid structure of arrays of generalized three legged elements. The technique he used is called the Mutual Impedance Method, which involves summing the mutual impedances from element to element in order to calculate array performance [2].

While Pelton was using the mutual impedance approach, Munk was working on another method of calculating properties of periodic surfaces called the Plane Wave Expansion Method [3]. This method also results in the mutual impedance sum, however it is obtained in a completely different manner. In the Plane Wave Expansion Method, the impedance sum is obtained by transforming the vector potential of an infinite array of incremental dipoles into an infinite series of plane waves by using the Poisson Sum Formula Transformation [4]. From these plane waves, the current induced by the array in a single reference element is calculated and an equivalent mutual impedance obtained. Once these impedances are found, it is an easy task to calculate the performance of the array.

Munk's Plane Wave Expansion Method can readily be applied to arrays of elements of arbitrary shape and to arrays imbedded in dielectric. However, it has only been applied to arrays with rectangular grid structure as in Figure 1. The objective of this report is to generalize this method in order to apply it to arrays with a skewed grid structure as shown in Figure 2. The results of this application will be presented, particularly in the case of an array of generalized three legged elements in a triangular grid structure. Arrays of this type play an important role in the design of metallic radomes.

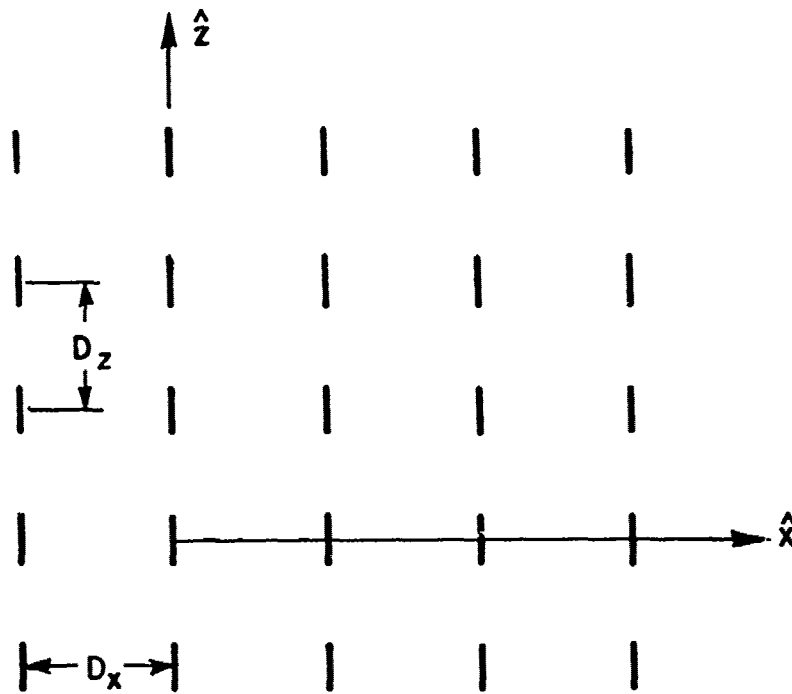


Figure 1. An array of straight dipoles having a rectangular grid structure.

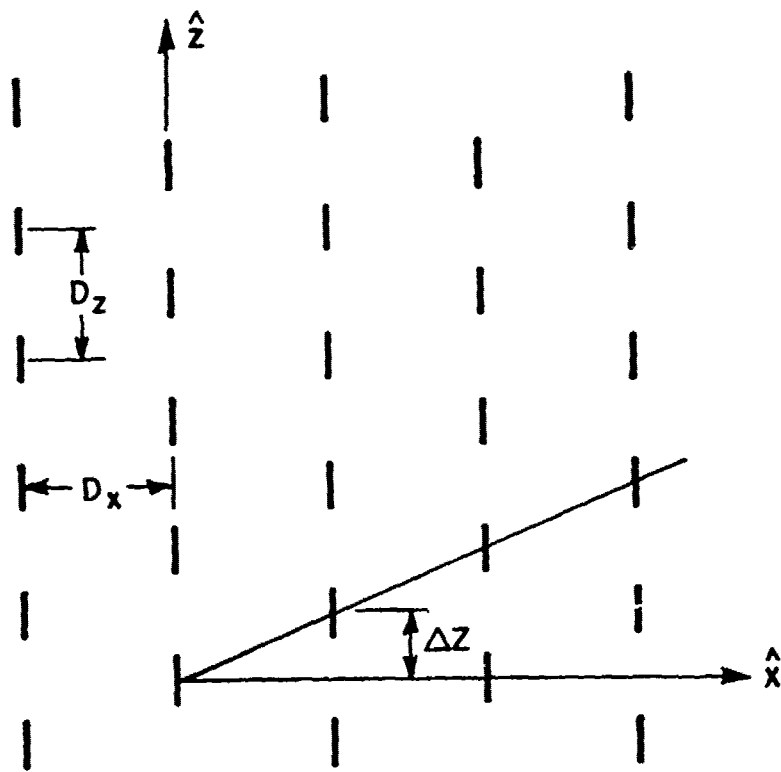


Figure 2. An array of straight dipoles having a skewed grid structure.

SECTION II DERIVATION

The first step in this analysis is to set up a skewed grid which satisfies the conditions necessary to apply the Poisson Sum Formula. The first condition is that the structure allows Floquet's Theorem to be used to determine the currents on each element. This means, simply, that each element is in the same environment as every other element or that, as one moves from element to element, all the surrounding elements are in the same relative locations. The grid structure in Figure 3 satisfies this condition. Secondly, the positions of the individual elements must be uniquely defined by two integer values. Using the integer variables q and m , the array element locations are uniquely defined by:

$$\begin{aligned}x &= q D_x \\z &= m D_z + q \Delta z\end{aligned}$$

where D_x, D_z , and Δz are constants and the array is located in the x - z plane. It is important to note that a number of arbitrary periodic grid structures can be realized by adjusting these three constants.

Now that the grid is set up, the spectrum of plane waves produced by this surface can be calculated. First, assume that dipoles of incremental length are located at each position in the array. As Munk has shown, the results can then be applied to more complex elements of almost any shape [5]. The vector potential from an individual dipole of incremental length, $d\ell$ can be written as

$$d\bar{A}_{qm} = \hat{p} \frac{\mu I_{qm} d\ell}{4\pi} \frac{e^{-j\beta r}}{r} \quad (1)$$

where \hat{p} is the unit vector defining the orientation of the dipole, I_{qm} is the current on the individual element, and r is the distance from the individual element to the point where the vector potential is desired. The propagation constant and permeability of the surrounding medium are denoted by β and μ , as usual.

By referring to Figure 3,

$$r = \sqrt{y^2 + (qD_x - x)^2 + (mD_z + q\Delta z - z)^2} \quad (2)$$

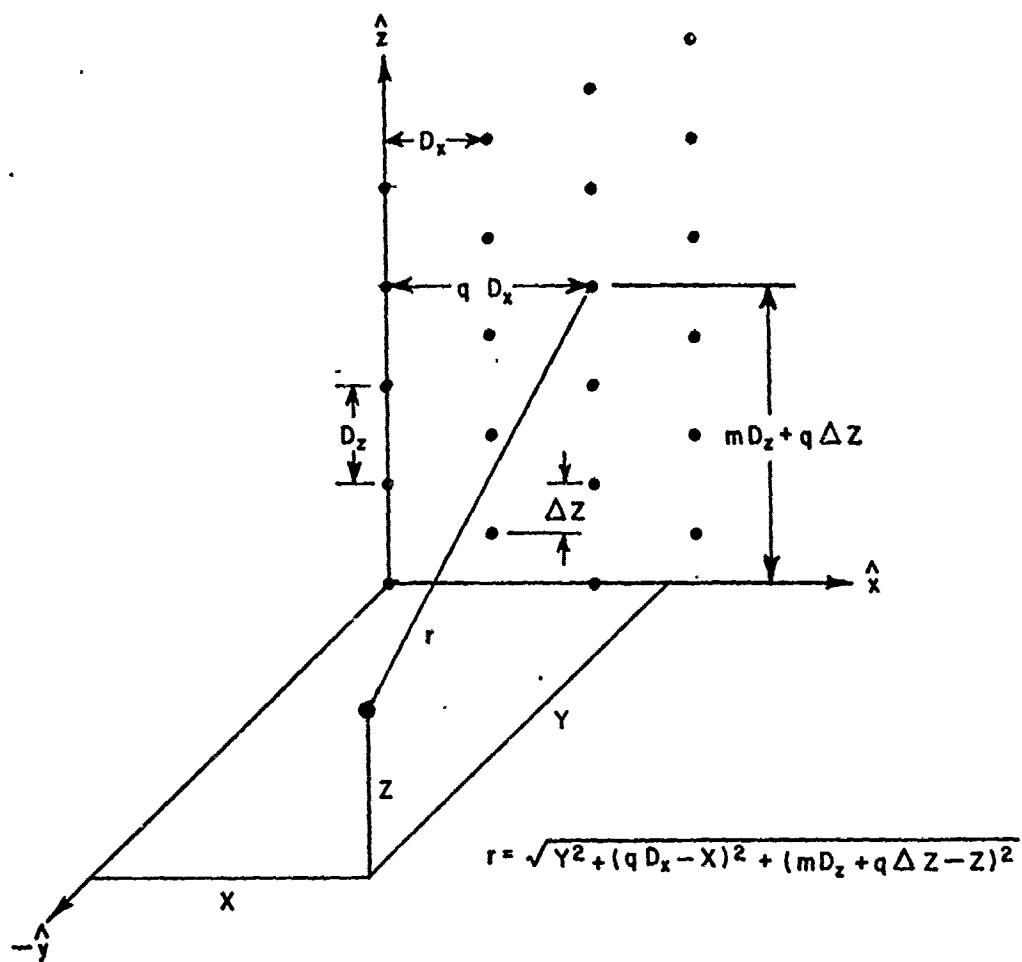


Figure 3. A view of the arbitrary grid structure to be considered, showing the parameters D_x , D_z and Δz .

where (x,y,z) define the observation point.

The currents I_{qm} can be found by assuming they are caused by an incident plane wave from the direction $r(i)_x \hat{x} + r(i)_y \hat{y} + r(i)_z \hat{z}$, where $r(i)_x$, $r(i)_y$, and $r(i)_z$ are the direction cosines of the propagation vector. Since they are caused by a plane wave, they vary only in phase (Floquet's Theorem). Thus

$$I_{qm} = I e^{-j\beta r(i)_x q D_x} e^{-j\beta r(i)_z (m D_z + q \Delta z)} \quad (3)$$

Using Equations (2) and (3) in (1), and summing over the infinite array,

$$\begin{aligned} d\vec{A} &= \sum_{q=-\infty}^{\infty} \sum_{m=-\infty}^{\infty} d\vec{A}_{qm} \\ &= \hat{p} \frac{\mu I d\ell}{4\pi} \sum_{q=-\infty}^{\infty} \sum_{m=-\infty}^{\infty} e^{-j\beta r(i)_x q D_x} e^{-j\beta r(i)_z (m D_z + q \Delta z)} \\ &\quad \frac{e^{-j\beta \sqrt{y^2 + (q D_x - x)^2 + (m D_z + q \Delta z - z)^2}}}{\sqrt{y^2 + (q D_x - x)^2 + (m D_z + q \Delta z - z)^2}} \end{aligned} \quad (4)$$

To handle this double summation, it will be arranged as the product of two summations by noting the fact that, while summing over m , q is constant and vice versa. Thus,

$$d\vec{A} = \hat{p} \frac{\mu I d\ell}{4\pi} \sum_{q=-\infty}^{\infty} e^{-j\beta q (r(i)_x D_x + r(i)_z \Delta z)} \sum_{m=-\infty}^{\infty} dA_m \quad (5)$$

where

$$\sum_{m=-\infty}^{\infty} dA_m = \sum_{m=-\infty}^{\infty} \frac{e^{-j\beta m r(i)_z D_z} e^{-j\beta \sqrt{a^2 + (m D_z + q \Delta z - z)^2}}}{\sqrt{a^2 + (m D_z + q \Delta z - z)^2}} \quad (6)$$

and $a^2 = y^2 + (q D_x - x)^2$ is constant for all m .

Equation (6) will now be transformed into an infinite series of different form by use of Poisson's Sum Formula and the Frequency Shifting Theorem [4].

Poisson's Sum Formula: [6]

$$\sum_{m=-\infty}^{\infty} e^{jm\omega_0 t} F(m\omega_0) = \frac{2\pi}{\omega_0} \sum_{n=-\infty}^{\infty} f\left(t + n \frac{2\pi}{\omega_0}\right) \quad (7)$$

where $f(t)$ and $F(\omega)$ are a Fourier Transform Pair.

Introducing the Frequency Shifting Theorem: [7]

$$e^{j\omega_1 t} f(t) \leftrightarrow F(\omega - \omega_1), \quad (8)$$

where ω_1 is any real constant, and combining (7) and (8), we get

$$\sum_{m=-\infty}^{\infty} e^{jm\omega_0 t} F(m\omega_0 - \omega_1) = \frac{2\pi}{\omega_0} \sum_{n=-\infty}^{\infty} e^{j\omega_1\left(t + n \frac{2\pi}{\omega_0}\right)} f\left(t + \frac{n2\pi}{\omega_0}\right) \quad (9)$$

Note the following Fourier Transform Pair: [8]

$$\frac{e^{-j\beta\sqrt{a^2 + \omega^2}}}{\sqrt{a^2 + \omega^2}} \leftrightarrow \left\{ -\frac{j}{2} H_0^{(2)}(a\sqrt{\beta^2 - t^2}) P_\beta(t) + \frac{1}{\pi} K_0(a\sqrt{t^2 - \beta^2})(1 - P_\beta(t)) \right\} \quad (10)$$

where the pulse function,

$$P_\beta(t) = \begin{cases} 1 & |t| < \beta \\ 0 & |t| > \beta \end{cases} .$$

Comparing Equation (10) to Equation (6) and the left hand side of (9), the following substitutions are suggested: Let $\omega_0 = D_z$, $t = -\beta r(i)_z$, and, since q is constant over the summation on m , $\omega_1 = z - q\Delta z$. Thus:

$$\sum_{m=-\infty}^{\infty} dA_m = \frac{2\pi}{D_z} \sum_{n=-\infty}^{\infty} e^{-j(z-q\Delta z)(\beta r(i)_z + n \frac{2\pi}{D_z})}$$

$$\left[-\frac{j}{2} H_0^{(2)} \left(a \sqrt{\beta^2 - \left(\beta r(i)_z + n \frac{2\pi}{D_z} \right)^2} \right) P_{\beta} \left(\beta r(i)_z + n \frac{2\pi}{D_z} \right) \right.$$

$$\left. + \frac{1}{\pi} K_0 \left(a \sqrt{\left(\beta r(i)_z + n \frac{2\pi}{D_z} \right)^2 - \beta^2} \right) \left(1 - P_{\beta} \left(\beta r(i)_z + n \frac{2\pi}{D_z} \right) \right) \right] \quad (11)$$

By noting that $\beta = 2\pi/\lambda$, carrying out the multiplication in the exponent, and combining with Equation (5),

$$d\vec{A} = \hat{p} \frac{\mu I d\ell}{4\pi} \frac{2\pi}{D_z} \sum_{q=-\infty}^{\infty} \sum_{n=-\infty}^{\infty} e^{-j\beta q(D_x r(i)_x + \Delta z r(i)_z)}$$

$$e^{-j\beta z \left(r(i)_z + n \frac{\lambda}{D_z} \right)} e^{j\beta q \left(\Delta z r(i)_z + \frac{n\Delta z \lambda}{D_z} \right)}$$

$$\left[-\frac{j}{2} H_0^{(2)}(a\beta s_1) P_{\beta}(t') + \frac{1}{\pi} K_0(a\beta s_1) (1 - P_{\beta}(t')) \right] \quad (12)$$

where $s_1 = \sqrt{1 - \left(r(i)_z + \frac{n\lambda}{D_z} \right)^2}$

$$t' = \beta \left(r(i)_z + \frac{n\lambda}{D_z} \right)$$

Simplifying further,

$$d\vec{A} = \hat{p} \frac{\mu I d\ell}{2D_z} \sum_{n=-\infty}^{\infty} e^{-j\beta z \left(r(i)_z + \frac{n\lambda}{D_z} \right)} \sum_{q=-\infty}^{\infty} dA_q \quad (13)$$

where

$$\sum_{q=-\infty}^{\infty} dA_q = \sum_{q=-\infty}^{\infty} e^{-j\beta q D_x \left(r(i)_x - \frac{n\Delta z \lambda}{D_x D_z} \right)}$$

$$\left[-\frac{j}{2} H_0^{(2)}(\alpha \beta s_1) P_\beta(t') + \frac{1}{\pi} K_0(\alpha \beta s_1) (1 - P_\beta(t')) \right]$$

Since n is constant over the summation on q , $\sum_{q=-\infty}^{\infty} dA_q$ can also be transformed by Poisson's Sum Formula. Remembering that $a^2 = y^2 + (qD_x - x)^2$,

$$\sum_{q=-\infty}^{\infty} dA_q = \sum_{q=-\infty}^{\infty} e^{-j\beta q D_x \left(r(i)_x - \frac{n\Delta z \lambda}{D_x D_z} \right)}$$

$$\left[-\frac{j}{2} H_0^{(2)}(\beta s_1 \sqrt{y^2 + (qD_x - x)^2}) P_\beta(t') + \frac{1}{\pi} K_0(j\beta s_1 \sqrt{y^2 + (qD_x - x)^2}) (1 - P_\beta(t')) \right] \quad (14)$$

Note the following Fourier Transform pairs: [9]

$$H_0^{(2)}(\beta s_1 \sqrt{y^2 + w^2}) \leftrightarrow \frac{e^{-jy \sqrt{(\beta s_1)^2 - t^2}}}{\sqrt{(\beta s_1)^2 - t^2}} \quad (15)$$

$$K_0(j\beta s_1 \sqrt{y^2 + w^2}) \leftrightarrow \frac{e^{-y\sqrt{t^2 - (\beta s_1)^2}}}{2\sqrt{t^2 - (\beta s_1)^2}} \quad (16)$$

Comparing Equations (14), (15), (16) and (9) suggests the following substitutions:

$$m=q, \omega_0=D_x, t = -\beta\left(r(i)_x - \frac{n\Delta z\lambda}{D_x D_z}\right), \omega_1 = x, \text{ and, to change the index of the summation, } k=m.$$

Thus

$$\sum_{q=-\infty}^{\infty} dA_q = \frac{2\pi}{D_x} \sum_{k=-\infty}^{\infty} e^{-jx\left(\beta\left(r(i)_x - \frac{n\Delta z\lambda}{D_x D_z}\right) + k \frac{2\pi}{D_x}\right)}$$

$$\left[-\frac{j}{2} \frac{e^{-jy\sqrt{(\beta s_1)^2 - \left(\beta\left(r(i)_x - \frac{n\Delta z\lambda}{D_x D_z}\right) + k \frac{2\pi}{D_x}\right)^2}}}{\pi \sqrt{(\beta s_1)^2 - \left(\beta\left(r(i)_x - \frac{n\Delta z\lambda}{D_x D_z}\right) + k \frac{2\pi}{D_x}\right)^2}} P_\beta(t') \right.$$

$$\left. + \frac{1}{\pi} \frac{e^{-y\sqrt{\left(\beta\left(r(i)_x - \frac{n\Delta z\lambda}{D_x D_z}\right) + k \frac{2\pi}{D_x}\right)^2 - (\beta s_1)^2}}}{2\sqrt{\left(\beta\left(r(i)_x - \frac{n\Delta z\lambda}{D_x D_z}\right) + k \frac{2\pi}{D_x}\right)^2 - (\beta s_1)^2}} (1-P_\beta(t')) \right] \quad (17)$$

This result can be simplified by using the following relationships:

$$\beta = \frac{2\pi}{\lambda}, s_1^2 = 1 - \left(r(i)_z + \frac{n\lambda}{D_z}\right)^2, \text{ and } \sqrt{A-B} = \sqrt{B-A}.$$

$$\sum_{q=-\infty}^{\infty} dA_q = \frac{2\pi}{D_x} \sum_{k=-\infty}^{\infty} e^{-j\beta x \left(r(i)_x + k \frac{\lambda}{D_x} - \frac{n\Delta z \lambda}{D_x D_z} \right)}$$

$$\left[\frac{-j}{2\pi\beta} \frac{e^{-j\beta y \sqrt{1 - \left(r(i)_z + \frac{n\lambda}{D_z} \right)^2 - \left(r(i)_x + \frac{k\lambda}{D_x} - \frac{n\Delta z \lambda}{D_x D_z} \right)^2}}}{\sqrt{1 - \left(r(i)_z + \frac{n\lambda}{D_z} \right)^2 - \left(r(i)_x + \frac{k\lambda}{D_x} - \frac{n\Delta z \lambda}{D_x D_z} \right)^2}} \right] \quad (18)$$

Finally, combining Equations (13) and (18)

$$d\bar{A} = -\hat{p} \frac{j\mu I d\ell}{2\beta D_x D_z} \sum_{n=-\infty}^{\infty} \sum_{k=-\infty}^{\infty} \left[e^{-j\beta x \left(r(i)_x + k \frac{\lambda}{D_x} - \frac{n\Delta z \lambda}{D_x D_z} \right)} \right]$$

$$\left[e^{-j\beta z \left(r(i)_z + n \frac{\lambda}{D_z} \right)} \right]$$

$$\left[\frac{e^{-j\beta y \sqrt{1 - \left(r(i)_x + k \frac{\lambda}{D_x} - n \frac{\Delta z \lambda}{D_x D_z} \right)^2 - \left(r(i)_z + n \frac{\lambda}{D_z} \right)^2}}}{\sqrt{1 - \left(r(i)_x + k \frac{\lambda}{D_x} - n \frac{\Delta z \lambda}{D_x D_z} \right)^2 - \left(r(i)_z + n \frac{\lambda}{D_z} \right)^2}} \right]$$

$$= -\hat{p} \frac{j\mu I d\ell}{2\beta D_x D_z} \sum_{n=-\infty}^{\infty} \sum_{k=-\infty}^{\infty} \frac{e^{-j\beta \vec{R} \cdot \hat{r}(k,n)}}{r(k,n)_y} \quad (19)$$

where

$$\hat{r}(k,n) = \hat{x} r(k,n)_x + \hat{y} r(k,n)_y + \hat{z} r(k,n)_z$$

Note that this resulting expression for the vector potential of an array of incremental dipoles is a doubly infinite sum of plane waves.

The sign of the square root in $r(k,n)_y$ must yet be determined. Rather than using mathematical arguments, the physical approach makes it easy to choose the right sign. As can be seen, $r(k,n)_y$ can be either real or imaginary. When it is real, it represents a wave propagating away from the array. When imaginary, it represents a wave which attenuates as it moves away from the array. From this argument, it has been found that, when the quantity under the radical is positive, the positive root is needed. When the quantity under the radical is negative, the $-j$ root is needed.

SECTION III
APPLICATION OF RESULTS

A. Straight Dipole Arrays

Comparing Equation (19) to the result obtained by Munk [3] for a rectangular grid, it can be seen that they differ only in the expression for $\hat{r}(k,n)$. For a rectangular grid,

$$\begin{aligned} \hat{r}(k,n) = \hat{x} \left(r(i)_x + k \frac{\lambda}{D_x} \right) \pm \hat{y} \sqrt{1 - r(k,n)_x^2 - r(k,n)_z^2} \\ + \hat{z} \left(r(i)_z + n \frac{\lambda}{D_z} \right) y \geq 0. \end{aligned} \quad (20)$$

Consequently, the final result of skewing the grid is simply the modification of the x and y components of the complex vector, $r(k,n)$. This fact makes the job of calculating the performance of arrays with a skewed grid structure very easy, since computer programs already exist for analyzing rectangular grid arrays.

It is interesting to note that the principal propagating mode (assuming no grating lobes) reflected by an array with rectangular grid structure is in the direction $\hat{r}(k,n)$ with $k = n = 0$ (i.e., $r(k,n)_y$ is real). Going back to $\hat{r}(k,n)$ for an arbitrary grid structure (Equation (19)) and comparing it to that for a rectangular grid (Equation (20)), it can be seen that, if $k = n = 0$, the two vectors are the same. This is a necessary condition which must be satisfied since the principal propagating mode must travel in the same direction regardless of grid structure.

When working with arrays of straight dipoles, it has been found that the real part of input impedance of an element in the array is determined by the $k=n=0$ term only (assuming no grating lobes) [10]. Since $\hat{r}(k,n)$ for $k=n=0$ is the same for both rectangular and skewed grids, only the imaginary part of the input impedance of an element in the array will differ in the two cases. The impedances shown in Figure 4 were obtained by modifying existing computer programs for analyzing arrays with a rectangular grid to include arrays having various amounts of skew. This figure depicts arrays consisting of z oriented dipoles. The real parts of the impedances are independent of grid structure for each incidence direction, as predicted above. However, a difference is noted in the imaginary parts as grid structure is varied. More explicitly, the maximum deviation from a rectangular grid structure is obtained when Δz is one half of D_z . Also, notice that the impedance

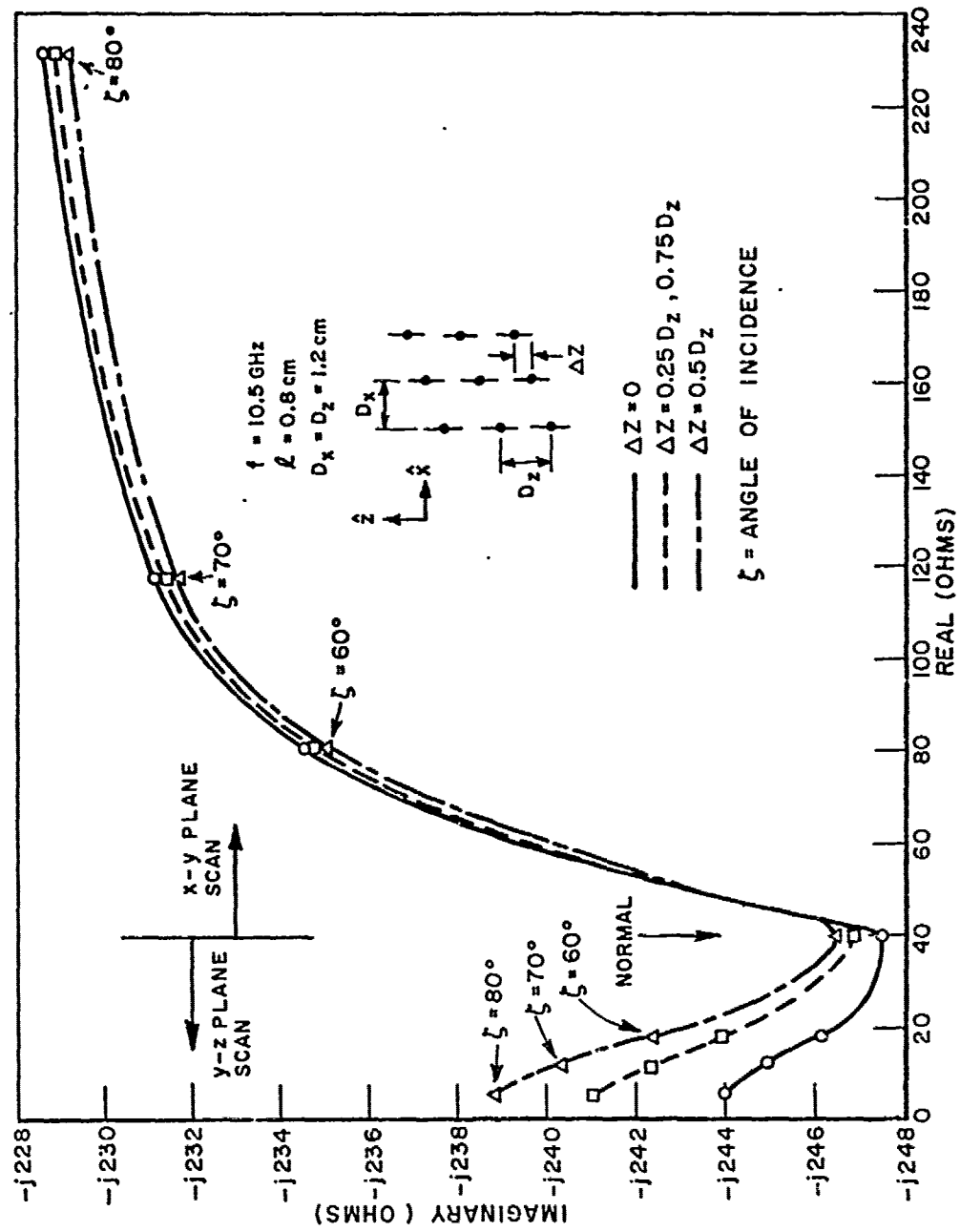


Figure 4. The input impedance of an element in an array of \hat{z} oriented dipoles having various amounts of skew. The angle of incidence, ζ is measured from the normal.

values obtained when $\Delta z = .25 D_z$ and $\Delta z = .75 D_z$ coincide. This is somewhat expected due to the periodicity of the array.

However, since the case where $\Delta z = .5 D_z$ yields the most variation from rectangular grid structure, it will be investigated further. Again, referring to Figure 4, it can be seen that, for scans in the y-z plane, the imaginary part becomes less negative. In the x-y plane, the change is negligible. This variation works to stabilize the resonant frequency of the reflection coefficient when scanning in the two planes. The stabilization is a result of the imaginary part of the impedance increasing for scans in the y-z plane, approaching the imaginary parts of the impedances observed for scans in the x-y plane. The curves in Figures 5 and 6, which, again, were obtained by adding Equation (19) to existing computer programs illustrate this effect for arrays of loaded z-oriented dipoles. In Figure 5, $\Delta z=0$ and in Figure 6, $\Delta z=.5D_z$.

B. Slot Arrays of Generalized Three Legged Elements

1. Background

Above, the effect of altering the grid structure of straight dipoles was discussed and possibilities for improved performance noted. This part of the report will deal with the investigation of slot arrays of generalized three legged elements. These elements are identical to those Pelton used in his investigation [11]. The motivation for using these elements is that they yield very good performance over all incident directions and polarizations. This property is essential in the design of metallic radomes. Briefly, generalized three legged elements consist of three connected monopoles having arbitrary length and direction ($\ell_1, \ell_2, \ell_3, \hat{p}_1, \hat{p}_2, \hat{p}_3$) as shown in Figure 7. Using this type of element and the arbitrary grid structure now available will allow the analysis of general periodic surfaces. Although the discussion which follows considers slot arrays of three legged elements in metal, the results apply to dipole arrays in free space having very thin elements (Babinet's Principle).

Before going into the analysis, some background information will be helpful. The performance of a surface will be rated with respect to the magnitude of the transmitted field parallel and orthogonal to the polarization of the incident field. The first magnitude (transmission) must be maximized and the second (cross component) minimized at the resonant frequency for all directions of incidence and polarizations. The appearance of a cross-polarized signal is the price paid for having good transmission for all incident polarizations. In contrast, for example, a straight dipole array will have no cross component when the incident field is aligned with the dipole, but no transmission when the incident field is orthogonal to the dipole.

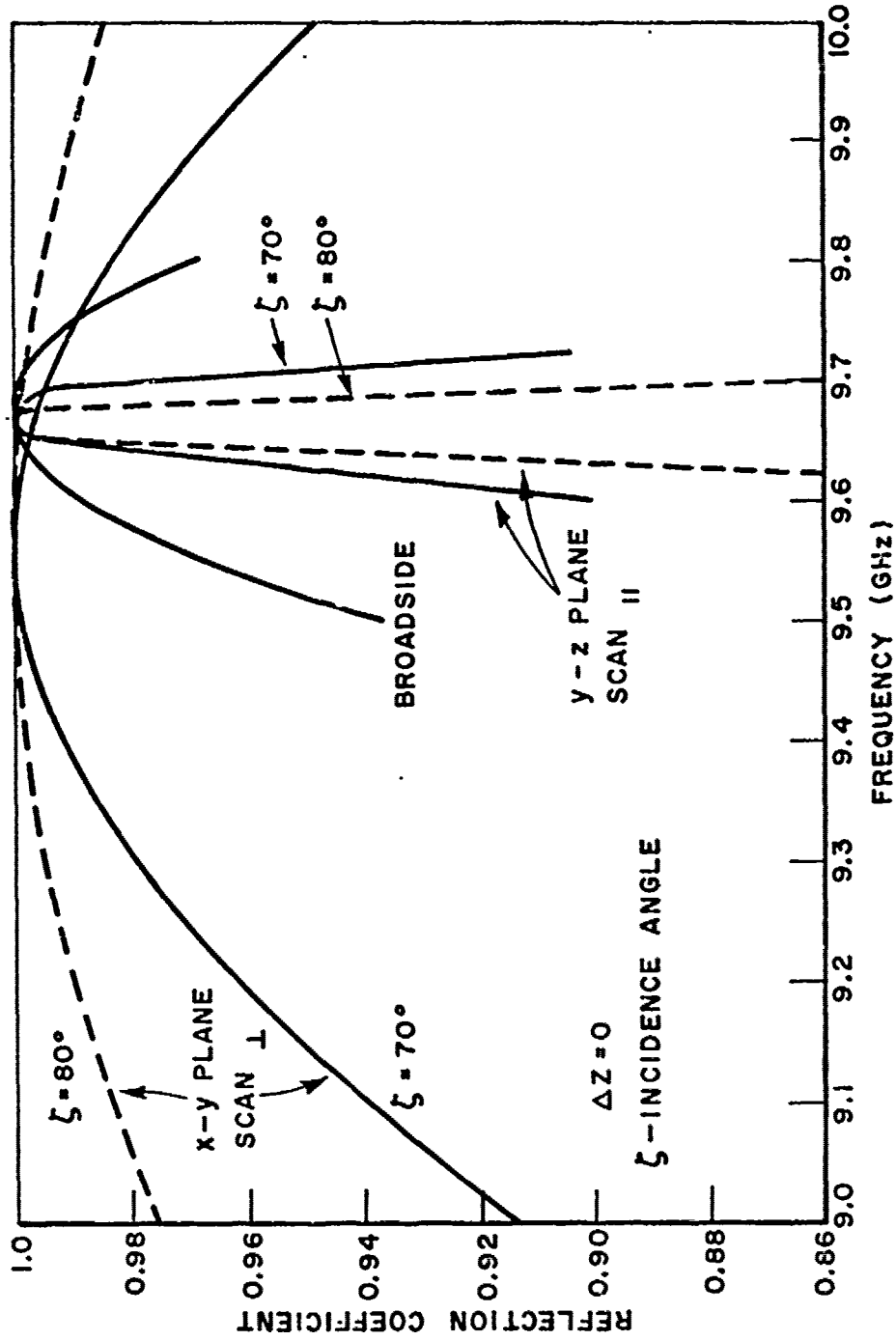


Figure 5. Reflection coefficient versus frequency for an array of \hat{z} oriented dipoles in a rectangular grid.

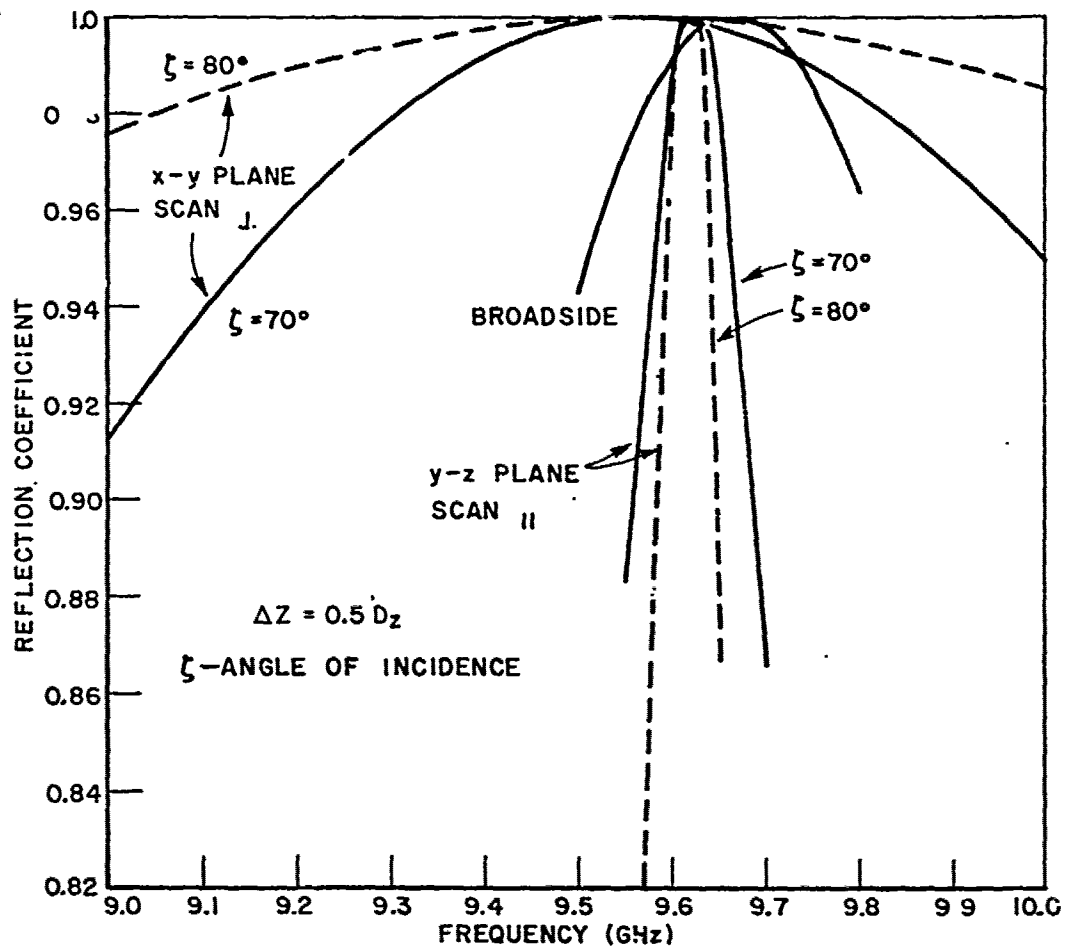


Figure 6. Reflection coefficient versus frequency for an array of \hat{z} oriented dipoles having a grid structure such that $\Delta z = .5 D_z$.

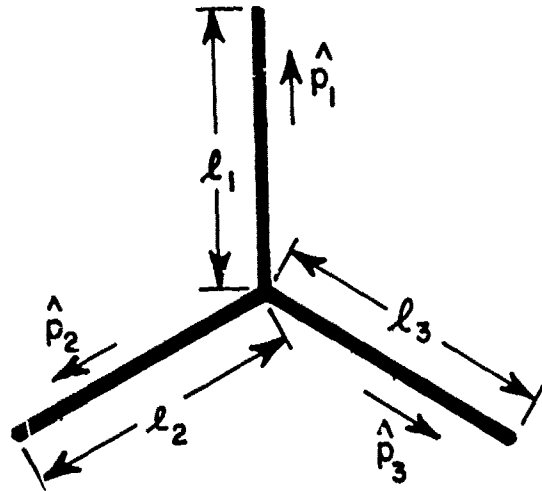


Figure 7. Generalized three legged element showing critical parameters.

The most obvious advantage of an arbitrary grid structure over a rectangular grid is that it allows closer packing of generalized three-legged elements as a result of individual element construction. Closer packing has been found to delay the onset of grating lobes (see Appendix A) and to stabilize the resonances for various incidence directions.

However, analysis beyond this simple physical observation requires a closer look at the mechanisms effecting the performance of an array. Munk has investigated the properties of arrays of generalized three legged elements (slots) having a rectangular grid structure [12]. Again, his findings can be modified to include a skewed grid structure simply by employing Equation (19). The properties of the admittances and element patterns mentioned below are discussed in detail in the reference cited directly above.

In his investigation, Munk assumes that two voltage modes are present on a slot when illuminated by a plane wave (symmetric and asymmetric modes), as shown in Figure 8. Assuming these modes, four admittances characteristic of the array are assumed: the mutual admittance of the all symmetric modes Y_{ss} , the mutual admittance of all asymmetric modes, Y_{aa} , and the admittances between the modes, Y_{as} and Y_{sa} . Munk found that the performance of an array in free space depends on the admittance sums obtained when the y-component of the vector $\hat{r}(k,n)$ (Equation (19)) is imaginary, (i.e., k and n both not equal to zero and no grating lobes) and on the pattern factor of an individual element. Because of this fact, each admittance is broken up into two terms:

$$\begin{aligned} Y_{ss} &= Y_{ss}^{00} + Y_{ss}^{\text{rest}} \\ Y_{aa} &= Y_{aa}^{00} + Y_{aa}^{\text{rest}} \\ Y_{as} &= Y_{as}^{00} + Y_{as}^{\text{rest}} \\ Y_{sa} &= Y_{sa}^{00} + Y_{sa}^{\text{rest}} \end{aligned}$$

Here, the superscript "00" denotes the admittance obtained from the $k=n=0$ term and the superscript "rest" denotes the sum of admittances for all other values of k and n. Munk's investigation determined that to obtain perfect transmission with no cross component for a specific frequency, polarization, and incidence direction it was necessary and sufficient to impose the following conditions:

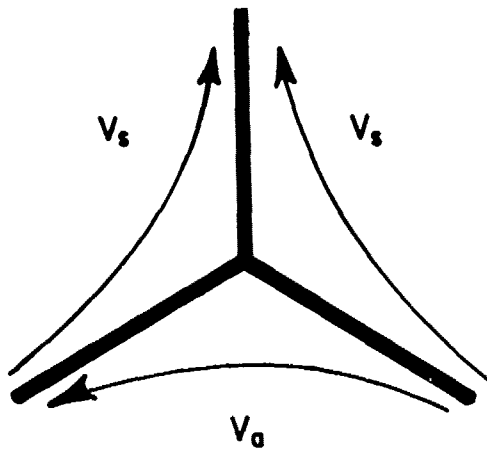


Figure 8. The voltage modes induced on a generalized three legged element.

For H-field parallel to plane of incidence

$$a) \gamma_{ss}^{\text{rest}} = \gamma_{sa}^{\text{rest}} \frac{\perp^P s}{\perp^P a} \quad (21a)$$

$$b) \gamma_{aa}^{\text{rest}} = \gamma_{as}^{\text{rest}} \frac{\perp^P a}{\perp^P s} \quad (21b)$$

for perpendicular polarization of the H-field,

$$a) \gamma_{ss}^{\text{rest}} = \gamma_{sa}^{\text{rest}} \frac{\parallel^P s}{\parallel^P a} \quad (22a)$$

$$b) \gamma_{aa}^{\text{rest}} = \gamma_{as}^{\text{rest}} \frac{\parallel^P a}{\parallel^P s} \quad (22b)$$

where

$$\left\{ \begin{array}{l} \perp \\ \parallel \end{array} \right\}^P \left\{ \begin{array}{l} a \\ s \end{array} \right\}$$

denotes the component of the element pattern perpendicular/parallel to the plane of incidence resulting from the asymmetric/symmetric voltage mode.

Analytically and by computer, certain relationships between the quantities in Equations (21) and (22) have been found to exist when the array is in free space [13]. The admittances $\gamma_{ss}^{\text{rest}}$ and $\gamma_{aa}^{\text{rest}}$ are always imaginary, while $\gamma_{as}^{\text{rest}}$, $\gamma_{sa}^{\text{rest}}$, and

$$\left\{ \begin{array}{l} \perp \\ \parallel \end{array} \right\}^P \left\{ \begin{array}{l} a \\ s \end{array} \right\}$$

are, in general, complex. This means that the complex quantities on the right hand sides of these equations must have a composite phase of $\pm 90^\circ$ before a unit transmission with no cross component can be achieved for a given frequency, polarization, and incidence direction. Further, it has been found that $\gamma_{as}^{\text{rest}}$ and $\gamma_{sa}^{\text{rest}}$ are negative complex conjugates when the array is in free space. Using this and the fact that the reciprocal of a complex number has the negative phase of the original number, it can be seen that, when the right hand side of 21a (22a) has a phase of $\pm 90^\circ$, the right hand side of 21b (22b) also has a phase of $\pm 90^\circ$. Moreover, as the right hand side of 21a (22a) approaches $\pm 90^\circ$ from one direction, the right hand side of 21b (22b) approaches $\pm 90^\circ$ at the same rate from the opposite direction in the complex plane.

Since the parallel and perpendicular components of the patterns are quite independent of each other in magnitude and phase, it becomes evident that, even though both parts of Equation (21) can be satisfied, it is not possible to satisfy Equation (22) at the same time, except in the trivial case of broadside incidence. Therefore, by this analysis, it can be seen that unit transmission with no cross component cannot be obtained for both polarizations given a specific frequency (resonance) and incidence direction. Up to now, no mention has been made of the magnitudes of the quantities in Equation (21) and (22). Here, it will suffice to note that once the correct phase is obtained, the magnitude of the left hand side can be changed relative to that of the right hand side, with little effect on the phase, by adjusting the length of the element legs. Again, this change will only yield perfect performance for one polarization. Consequently, the best over-all performance will be a compromise with "acceptable" values of transmission and cross components for all polarizations and incidence directions.

Having set forth this background for the problem at hand, the objective of this part of the report can now be explored; that is, to find the effect of grid structure on the performance of arrays of generalized three legged elements. An additional restriction placed on this objective is that it lead to a family of grid/element combinations yielding good performance as described above.

To date, the best performance has been obtained from an array of closely packed elements with 120° between the legs arranged in an equilateral triangular grid as shown in Figure 9 [14]. An array designed in this manner produces a transmitted field with a low cross component when scanning in planes which coincide with the legs, ($\alpha = 30^\circ, 90^\circ$, etc.) and higher, but not unbearable cross components when scanning in planes which bisect the legs ($\alpha = 0^\circ, 60^\circ$, etc.) Also, closely packed grid structure tends to stabilize the resonances of transmission with respect to frequency, polarization, and direction of incidence. Figure 10 depicts the performance of such an array for an incidence angle of 60° with the normal. It is evident that the parallel and perpendicular resonances are not very stable. As mentioned above, stability is obtained by close packing of the elements. In real life, the elements may be packed closer together, but on the existing computer analysis, any closer packing will result in erroneous results, due to certain assumptions made about the voltage modes existing on the elements. In practice, closer packing may also be obtained by using loaded three legged elements [15], and by imbedding the array in dielectric [16]. The mutual admittances in Equations (21) and (22) have been calculated for this array, and will be discussed later in this report.

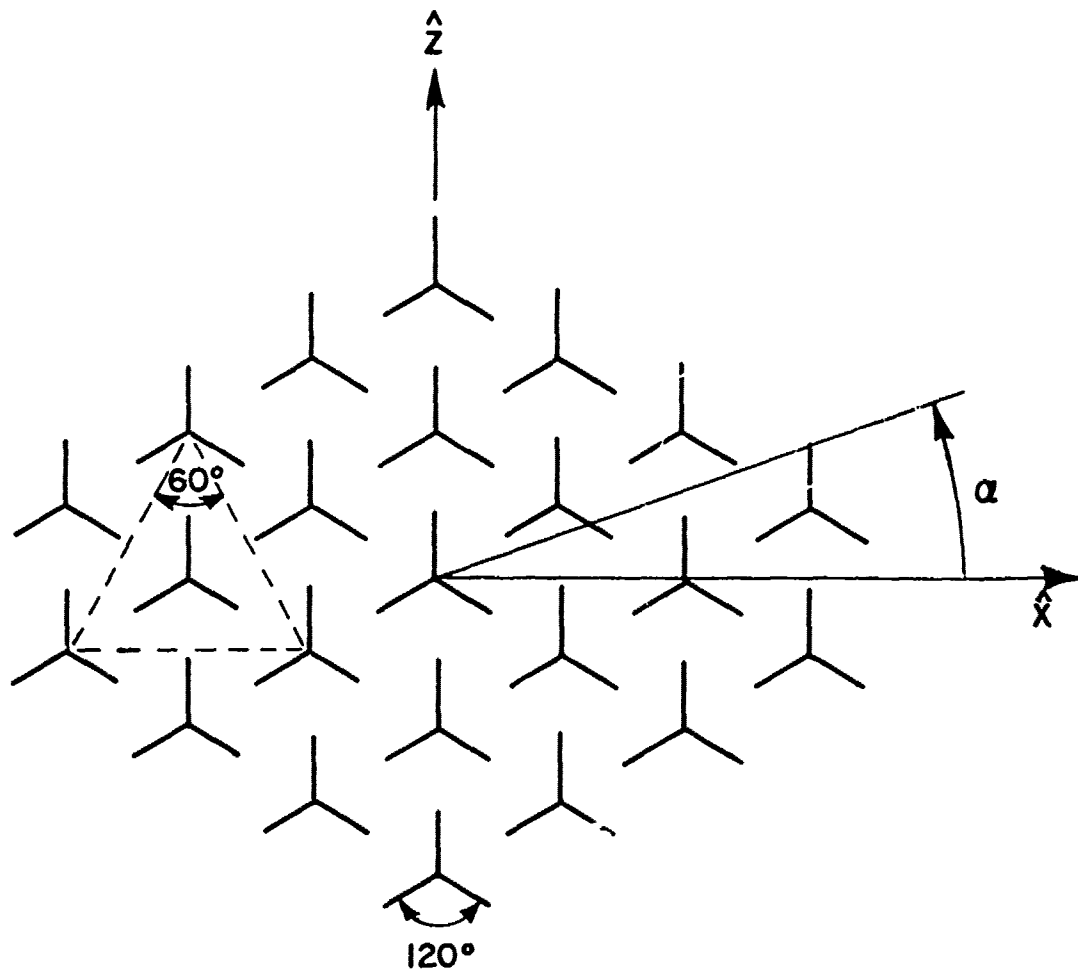


Figure 9. Portion of an equilateral triangular grid array with 120° between the element legs. Also, the angle α which defines the plane of incidence.

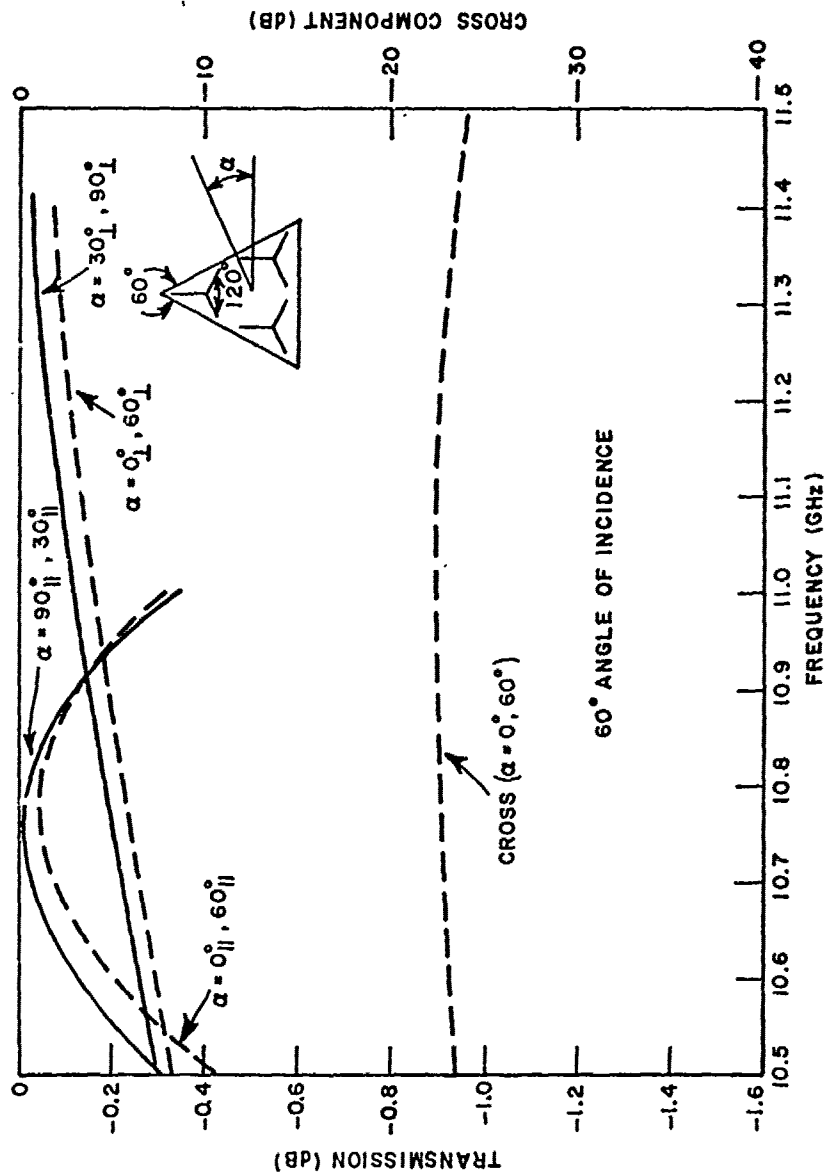


Figure 10. Magnitudes of the transmitted field (left scale) and cross component (right scale versus frequency for a slot array having an equilateral triangular grid and 120° between the element legs. The symbols (\parallel) denote the H-field (parallel/perpendicular) to the plane of incidence defined by α .

The author has found that, given an equilateral triangular grid, a 120° leg angle yields the best performance yet obtained. Since this array yields favorable and predictable results, it will serve as a benchmark against which to compare other arrays.

Here a question arises. If this grid/element combination is so good, why change it? The problem stems from the fact that an equilateral triangular grid is not compatible with current radome designs [17]. Therefore the grid structure will depend on each individual radome, and the element configuration must be changed to optimize the performance of the surface.

2. Optimum Grid-Element Combinations

The discussion which follows will assume a fixed incidence angle of 60° with the normal and the performance will be noted with respect to plane of incidence (α in Figure 9), frequency, and polarization. It has already been pointed out that perfect performance cannot be expected for all incidence planes and both polarizations at the same frequency.

Figure 11 depicts the structure of an array of generalized three legged elements. The points in this figure represent the centers of the elements (a representative element is shown). For the equilateral triangle case described above, the side grid angle (SGA) is 60° , the top grid angle (TGA) is 60° , and the leg angle (LA) is 120° . The grid angle is the quantity which must be changed for universal radome applications. Appendix B shows the relationship between the top and side grid angles.

The investigation will proceed as follows. First a particular grid angle is picked. The inter-element spacing adjusted in such a way that the product $D_x D_z$ is the same as in the equilateral triangular grid case (see Equation (19)). Then the leg angle will be adjusted to optimize the array performance. It has been found that having a leg aligned along the z axis yields the best performance, therefore the leg angle will be the only element structure variable.

The first grid angle investigated was a top grid angle of 55° . Figures 12 through 14 illustrate the performance of arrays with TGA= 55° and LA = 120° , 110° , 105° . By comparing the transmission curves, it can be seen that there is minimal change in the broad resonance for perpendicular polarization. Table 1 summarizes transmission and cross components for parallel polarization. (By reciprocity, the cross component for both polarizations is the same.) By consulting Table 2 and the transmission curves (note the scale!), it can be seen that the transmission performance of the arrays is relatively unaffected. However, the cross components tell a different story. In the equilateral case, the cross component was -22.5 dB in both the $\alpha = 0^\circ$ and 60° planes, and for all purposes nonexistent in the $\alpha=30^\circ$

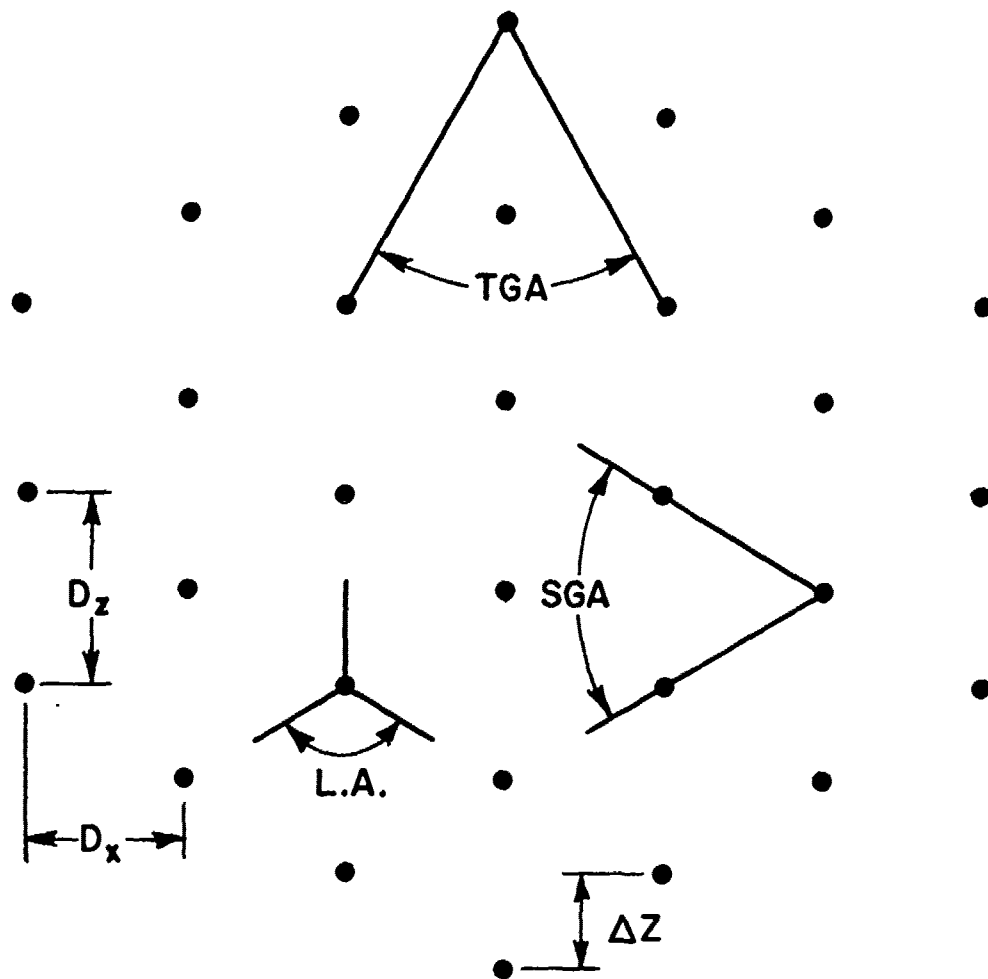


Figure 11. Grid structure depicting the variables involved with the investigation: top grid angle (TGA), side grid angle (SGA), leg angle (LA), and D_x , D_z and Δz , the array parameters.

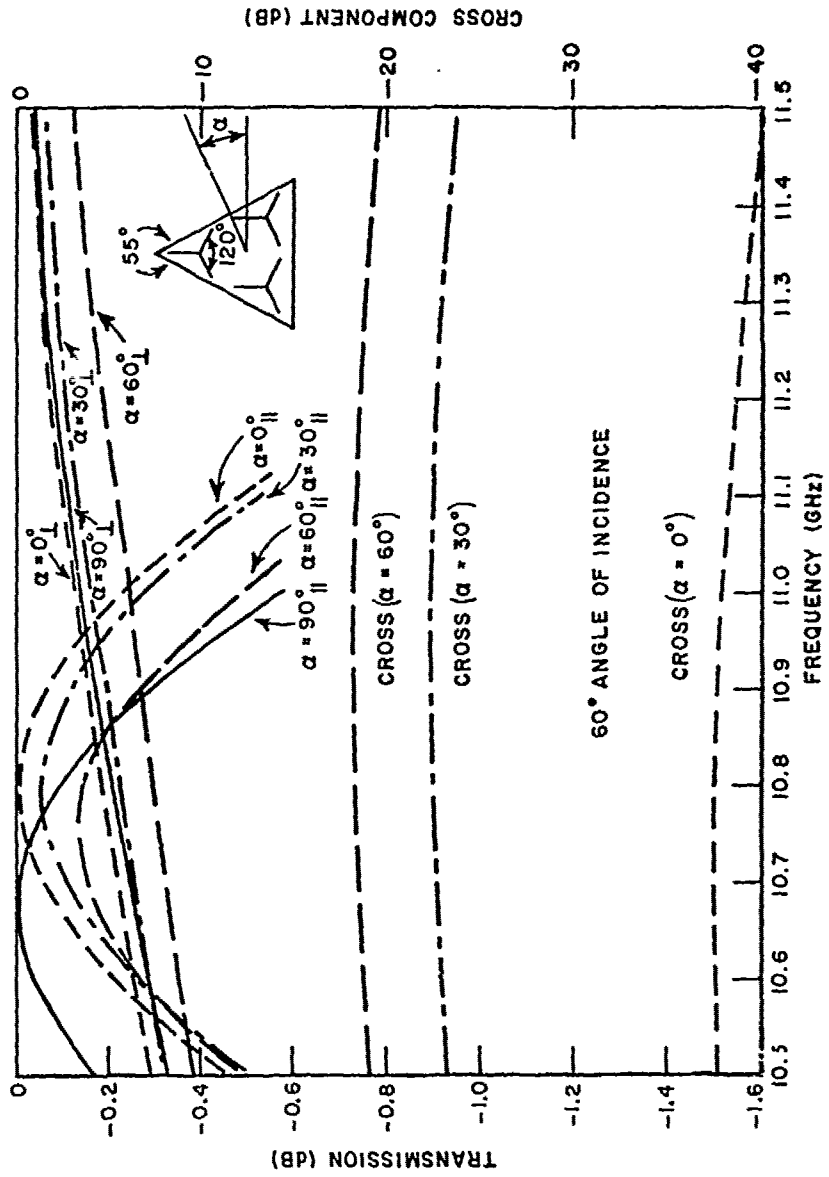


Figure 12. Magnitudes of the transmitted field (left scale) and cross component (right scale) versus frequency for the 55/120 (TGA/LA) slot array. The symbols (\parallel/\perp) denote the H-field (parallel/perpendicular) to the plane of incidence defined by α .

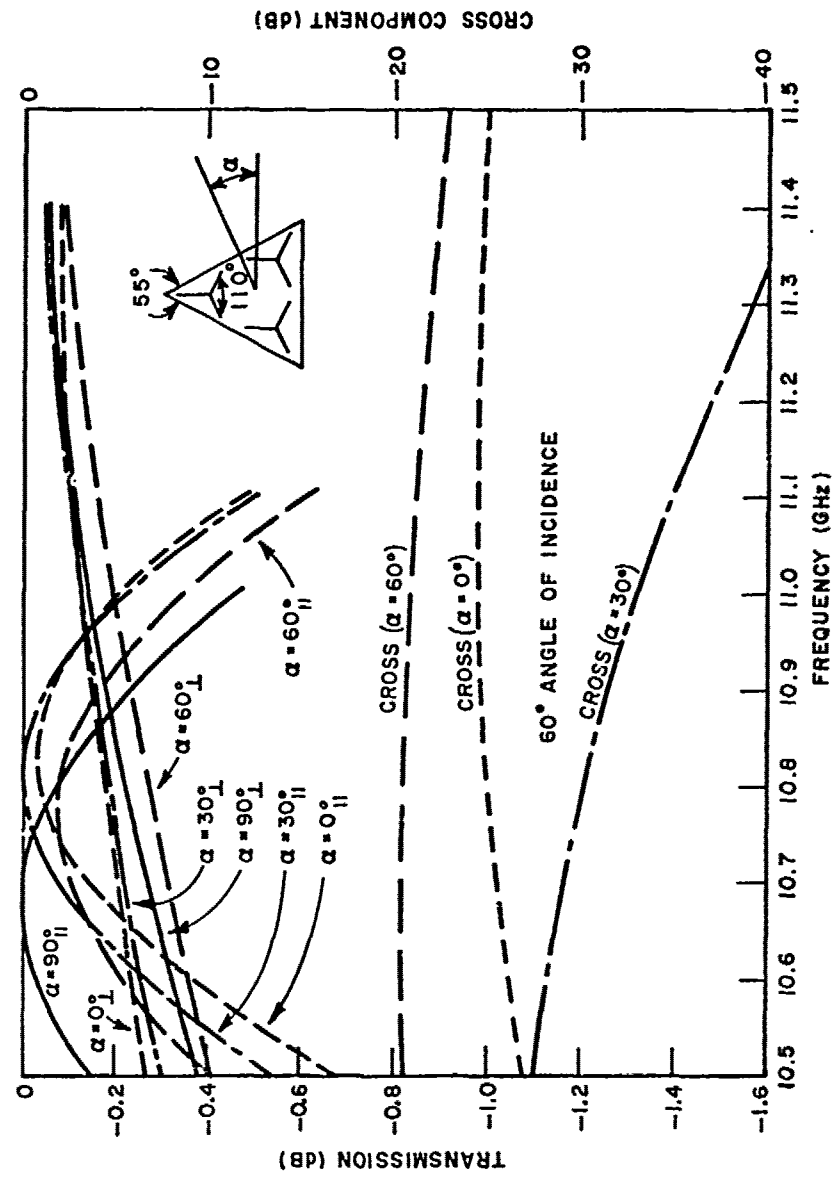


Figure 13. Magnitudes of the transmitted field (left scale) and cross component (right scale) versus frequency for the 55/110 (TGA/LA) slot array. The symbols (\parallel / \perp) denote the H-field (parallel/perpendicular) to the plane of incidence defined by α .

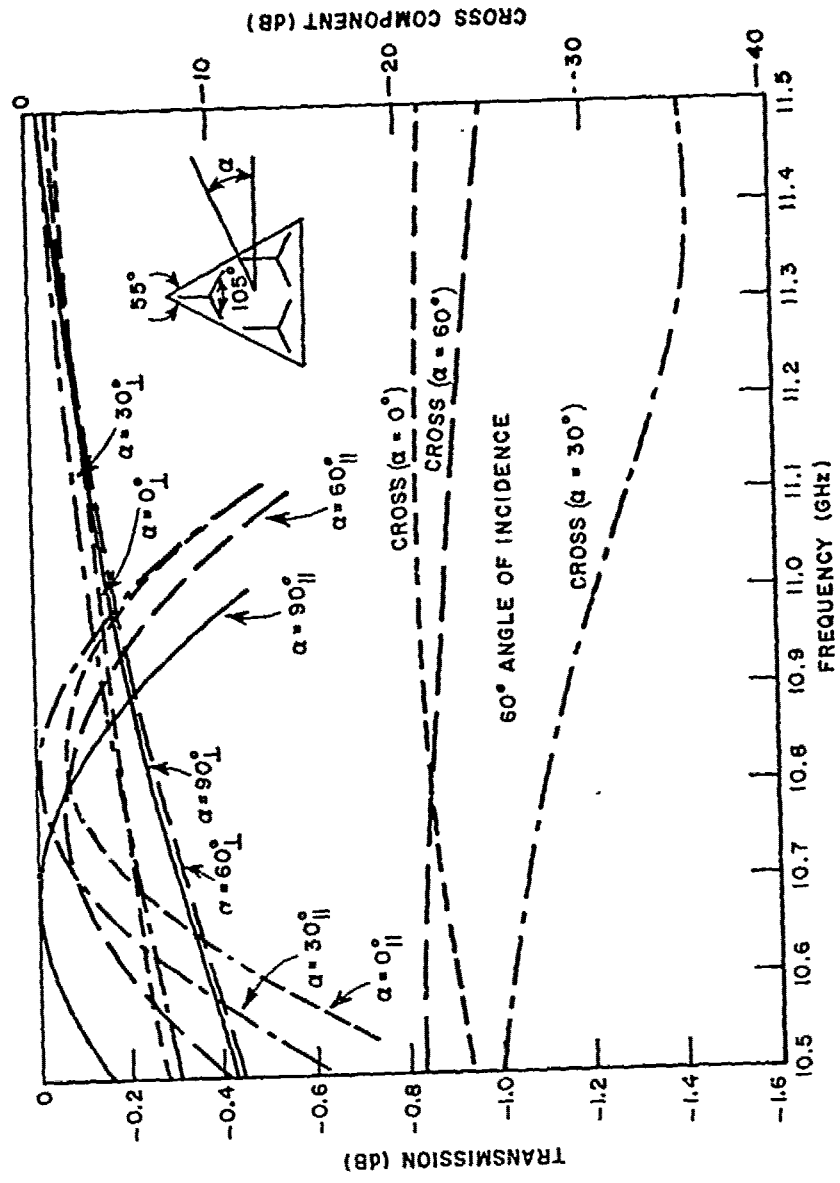


Figure 14. Magnitudes of the transmitted field (left scale) and cross component (right scale) versus frequency for the 55/105 (TGA/LA) slot array. The symbols (\parallel / \perp) denote the H-field (parallel/perpendicular) to the plane of incidence defined by α .

TABLE 1
Comparison of various elements (LA) in arrays with TGA=60° and 55°.

TGA	LA	Resonant Frequency GHz				Loss dB				Cross at Resonance dB			
		$\alpha=0^\circ$	30°	60°	90°	0°	30°	60°	90°	0°	30°	60°	90°
60°	120°	10.8	10.75	10.8	10.75	.05	0	.05	0	-22.5	-70	-22.5	-∞
55°	120°	10.8	10.8	10.8	10.7	0	.05	.14	0	-37	-22.5	-18	-∞
55°	110°	10.8	10.8	10.8	10.7	.03	.01	.08	0	-25	-30	-20.5	-∞
55°	105°	10.85	10.8	10.8	10.7	.07	.02	.07	0	-21.5	-27.5	-21.5	-∞

TABLE 2
Comparison of various elements (LA) in arrays with TGA=60° and 65°.

TGA	LA	Resonant Frequency GHz				Loss dB				Cross at Resonance dB			
		$\alpha=0^\circ$	30°	60°	90°	0°	30°	60°	90°	0°	30°	60°	90°
60°	120°	10.8	10.75	10.8	10.75	.05	0	.05	0	-22.5	-70	-22.5	-∞
65°	120°	10.8	10.7	10.8	10.8	.23	.05	.02	0	-16	-22.5	-28	-∞
65°	135°	10.75	10.7	10.8	10.85	.07	.02	.06	0	-21.5	-29	-21.5	-∞

and 90° plane. As soon as the grid angle is changed, the cross at $\alpha=60^\circ$ rises to -18 dB. At $\alpha=30^\circ$, it goes up to -22.5 dB and at $\alpha=0^\circ$ it was down to -37 dB (at $\alpha=90^\circ$, it will always be zero). By increasing the leg angle, the cross at $\alpha=60^\circ$ can be brought back down, at the price of moving the cross at $\alpha=0^\circ$ up. The optimum performance then, was decided to be where the cross for $\alpha=0^\circ$ and $\alpha=60^\circ$ is the same, at the resonance for parallel polarization. From Figure 14, this occurs when the leg angle is 105° , where the cross is -21.5 dB in both cases

Figures 15 and 16 and Table 2 summarize the results of the same test for T.G.A. = 65° . In this case, when the grid angle is changed and the leg angle remains at 120° , the cross in the $\alpha=0^\circ$ plane rises drastically, while that in the $\alpha=60^\circ$ plane is decreased. By making the leg angle 135° , the cross components in both planes may again be equalized at -21.5 dB. Earlier, it was mentioned that adjusting the leg length might be advantageous when trying to achieve optimum performance. This possibility has not been investigated at this time.

Accordingly, a family of three grid/element combinations leading to good performance has been found: (TGA/LA), 60/120, 55/105, 65/135. In the course of finding this family, many important effects of grid structure on array performance have been found. First, as has been expected, the 60/120 combination involves a certain symmetry which cannot be repeated for any other array design. This symmetry is evident in the array's performance since the array repeats itself every $\alpha=60^\circ$. Changing the grid has a slight effect on the resonant frequency and the loss in transmission at resonance. The real difference is seen by observing the cross component. Of course, in the $\alpha=90^\circ$ plane, the cross component is always zero due to the symmetry of each element. However, in the other planes of incidence, the change in cross component is very evident. When the TGA is increased, the cross component increases in the $\alpha=30^\circ$ and $\alpha=0^\circ$ planes and decreases in the $\alpha=60^\circ$ plane. When the TGA is decreased, the cross component increases in the $\alpha=30^\circ$ and $\alpha=60^\circ$ planes and decreases in the $\alpha=0^\circ$ plane. The leg angle, then, is adjusted to equalize the cross in both planes and achieve the optimum performance. The change in cross component is also evident in the transmitted field. When the cross component in a particular plane of incidence increases, the magnitude of the transmitted field falls further below unity. Finally, the slight shift in resonance frequency in the $\alpha=0^\circ$ and $\alpha=90^\circ$ planes can be explained. In order to optimize performance, the leg angle must be changed. As the leg angle is increased, each element appears longer in the $\alpha=0^\circ$ plane (resonance frequency decreases) and shorter in the $\alpha=90^\circ$ plane (resonance frequency increases). The opposite is true when the leg angle is decreased.

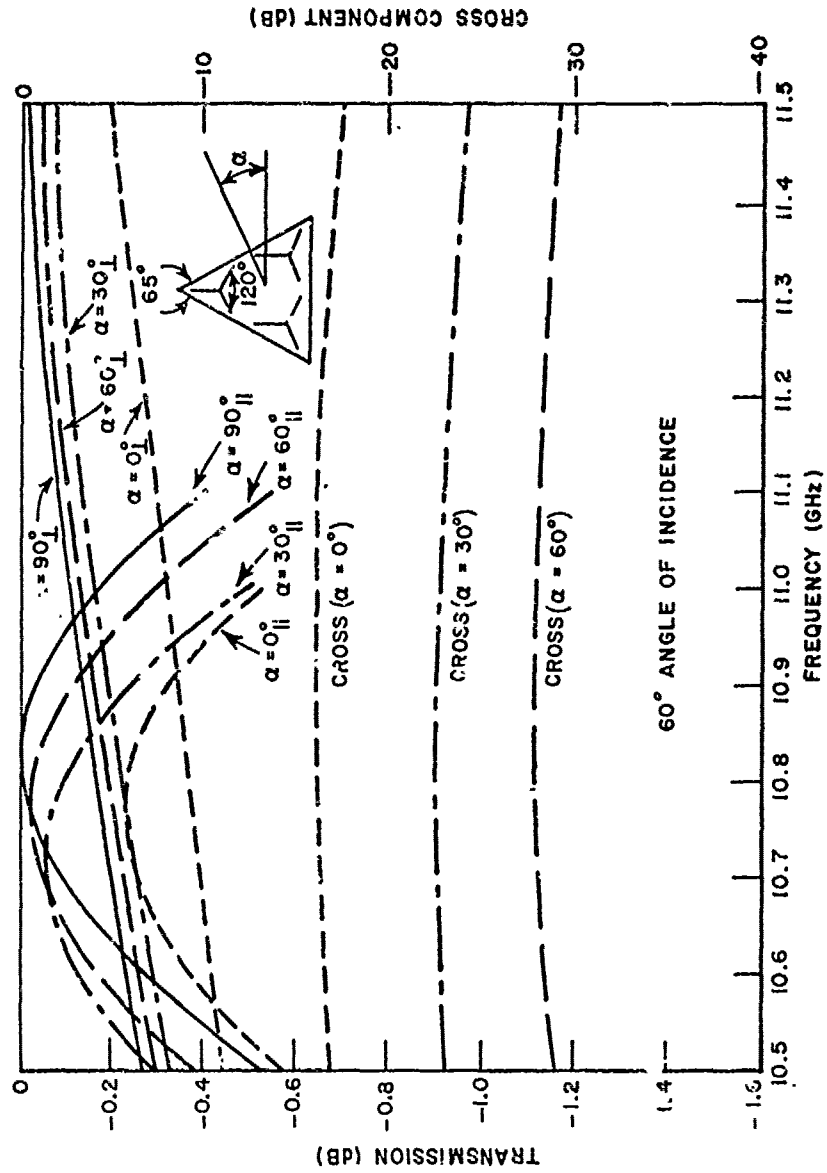


Figure 15. Magnitudes of the transmitted field (left scale) and cross component (right scale) versus frequency for the 65/120 (TGA/LA) slot array. The symbols (\parallel / \perp) denote the H-field (parallel/perpendicular) to the plane of incidence defined by α .

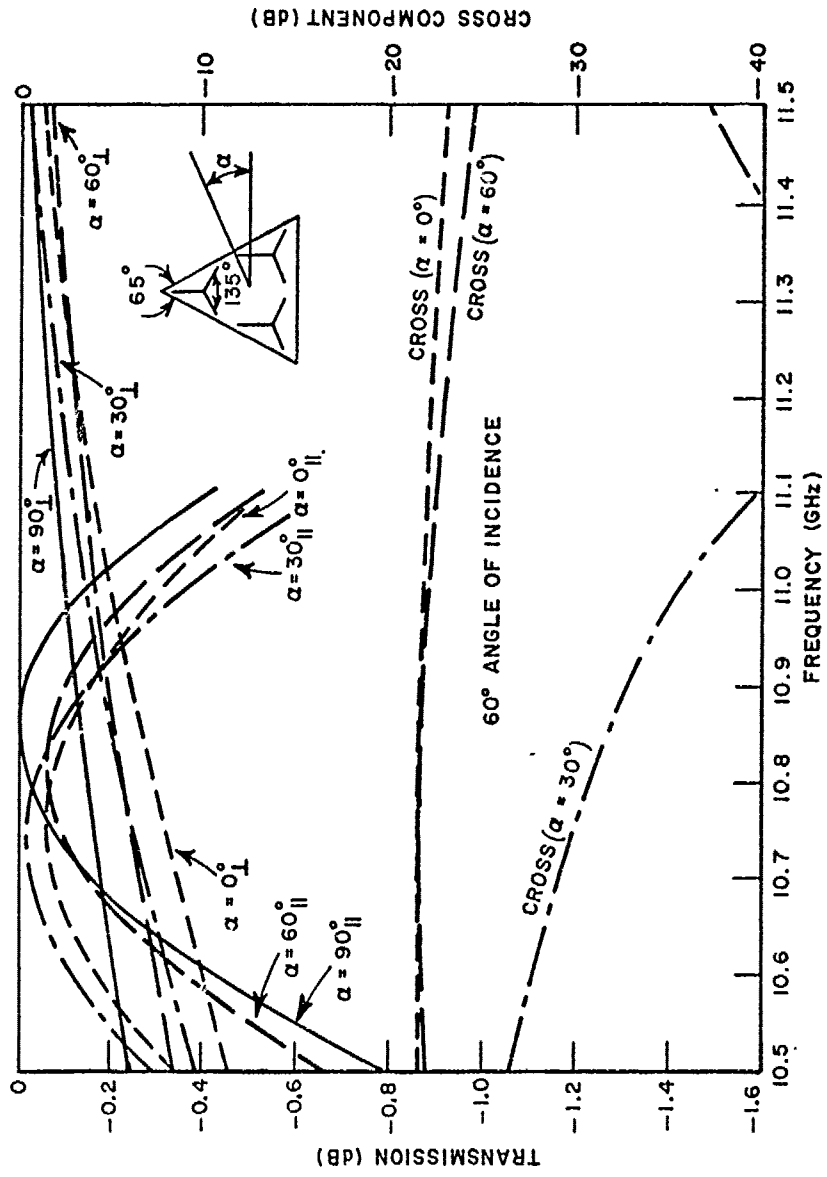


Figure 16. Magnitudes of the transmitted field (left scale) and cross component (right scale) versus frequency for the 65/135 (TGA/LA) slot array. The symbols (\parallel / \perp) denote the H-field (parallel/perpendicular) to the plane of incidence defined by α .

Arrays yielding good performance are centered about the 60/120 array. It can be seen in the cases cited above and has been found in other cases that, when the top grid angle deviates from 60°, optimum performance is maintained by changing the leg angle by approximately three times as much, i.e.,

$$LA \approx 120^\circ + 3 (TGA - 60^\circ) \quad (23)$$

To date, top grid angles between 55° and 65° have been investigated. In this range, the above equation is valid. For deviations of more than 5°, the factor of three tends to become closer to 3.2. The upper limit of allowable deviation has not been investigated.

3. Analysis of Results

As inspection of Equations (21) and (22) show, the keys to the performance of an array of generalized three legged elements are the admittances, Y_{ss}^{rest} , Y_{aa}^{rest} , Y_{as}^{rest} , Y_{sa}^{rest} , and the pattern factors,

$$\begin{Bmatrix} I \\ II \end{Bmatrix}^P \begin{Bmatrix} a \\ s \end{Bmatrix}$$

Changing the grid structure of an array has no effect on the pattern factors, but changing the leg angle changes the pattern factors and the admittances. Figures 17 through 20 show the pattern factor for elements having leg angles of 105° and 135°. The patterns shown are for various incidence planes at a 60° incidence angle. Although some variation can be seen, note that the two sets of curves represent the two extremes of leg angles which were used. Figures 21 and 22 show the magnitude of the admittances Y_{ss}^{rest} and Y_{aa}^{rest} for 60/120, 55/120, and 65/120 arrays. In these figures, the incidence angle is 60° with the normal and the frequency is slightly below resonance. The phase is -90° for all cases. In addition, the admittances for 60/105 and 60/135 arrays fall in the same range as those in the figures, but were omitted to preserve the clarity of the figures. The relative invariance of the admittances Y_{ss}^{rest} and Y_{aa}^{rest} and the patterns for the extreme cases considered above leads to the assumption that the admittances Y_{as}^{rest} and Y_{sa}^{rest} are the primary factors affecting array performance. Accordingly, these admittances will be studied in depth in the pages to follow.

Figure 23 shows the admittance Y_{as}^{rest} for the 60/120 array slightly below resonance. This admittance is related to Y_{sa}^{rest} by: $Y_{sa}^{rest} = -Y_{as}^{rest*}$ for an array in free space [18]. These figures are quite a shock, since up to this point it was thought that the mutual admittance had to be zero for optimum performance.

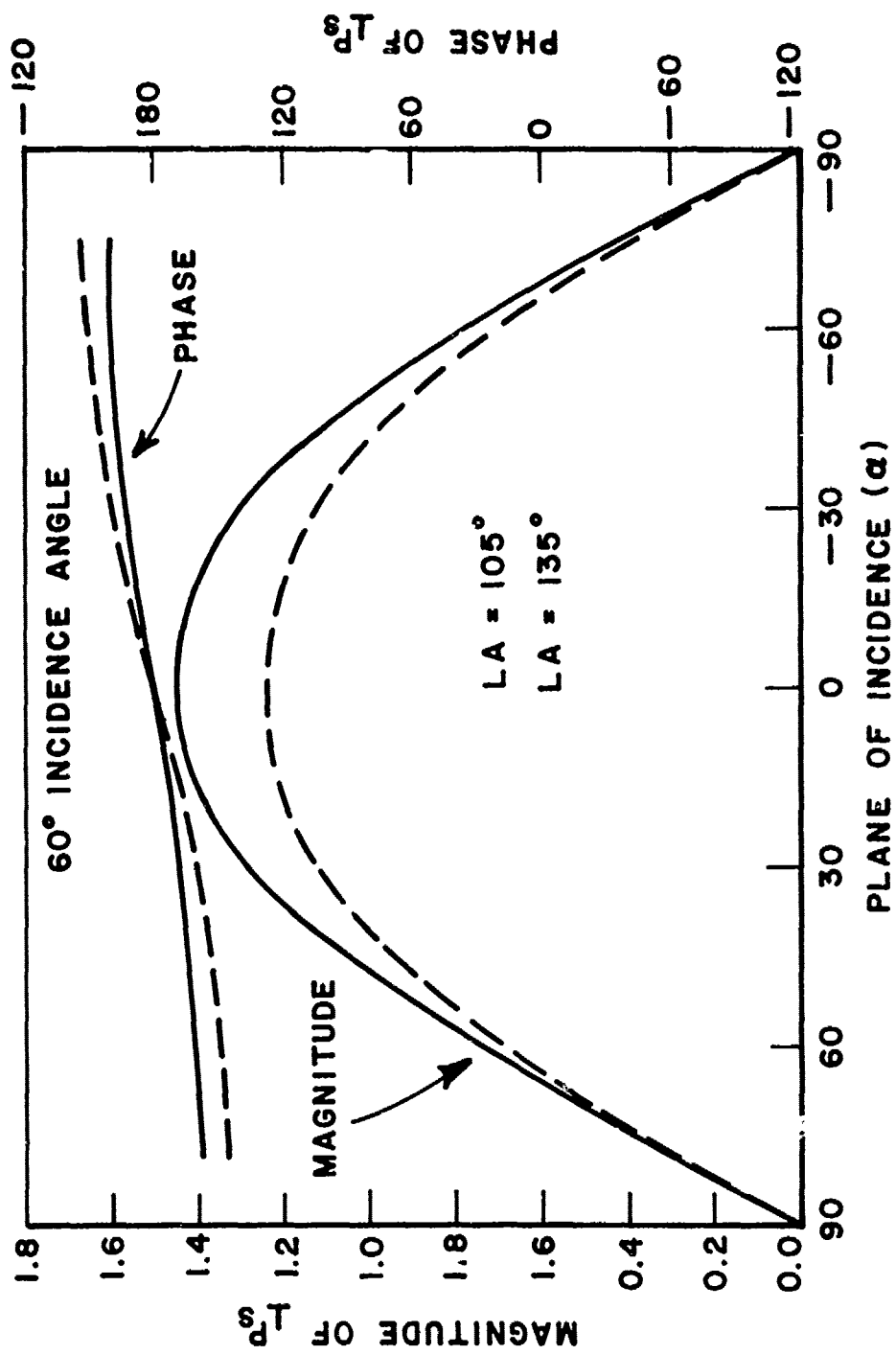


Figure 17. Perpendicular component of the pattern factor of the symmetric voltage mode for leg angles of 105° and 135° .

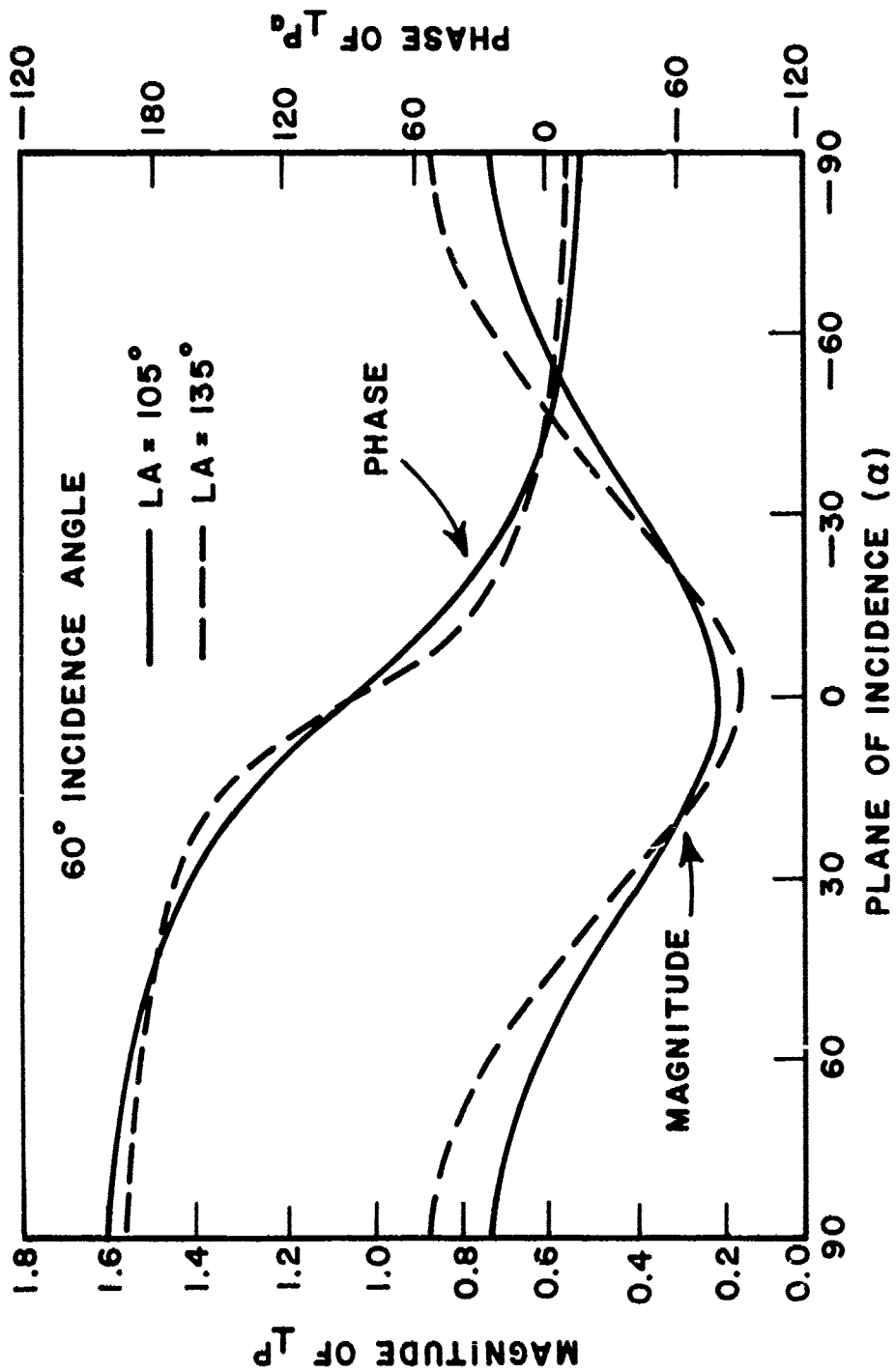


Figure 18. Perpendicular component of the pattern factor of the asymmetric voltage mode for leg angles of 105° and 135°.

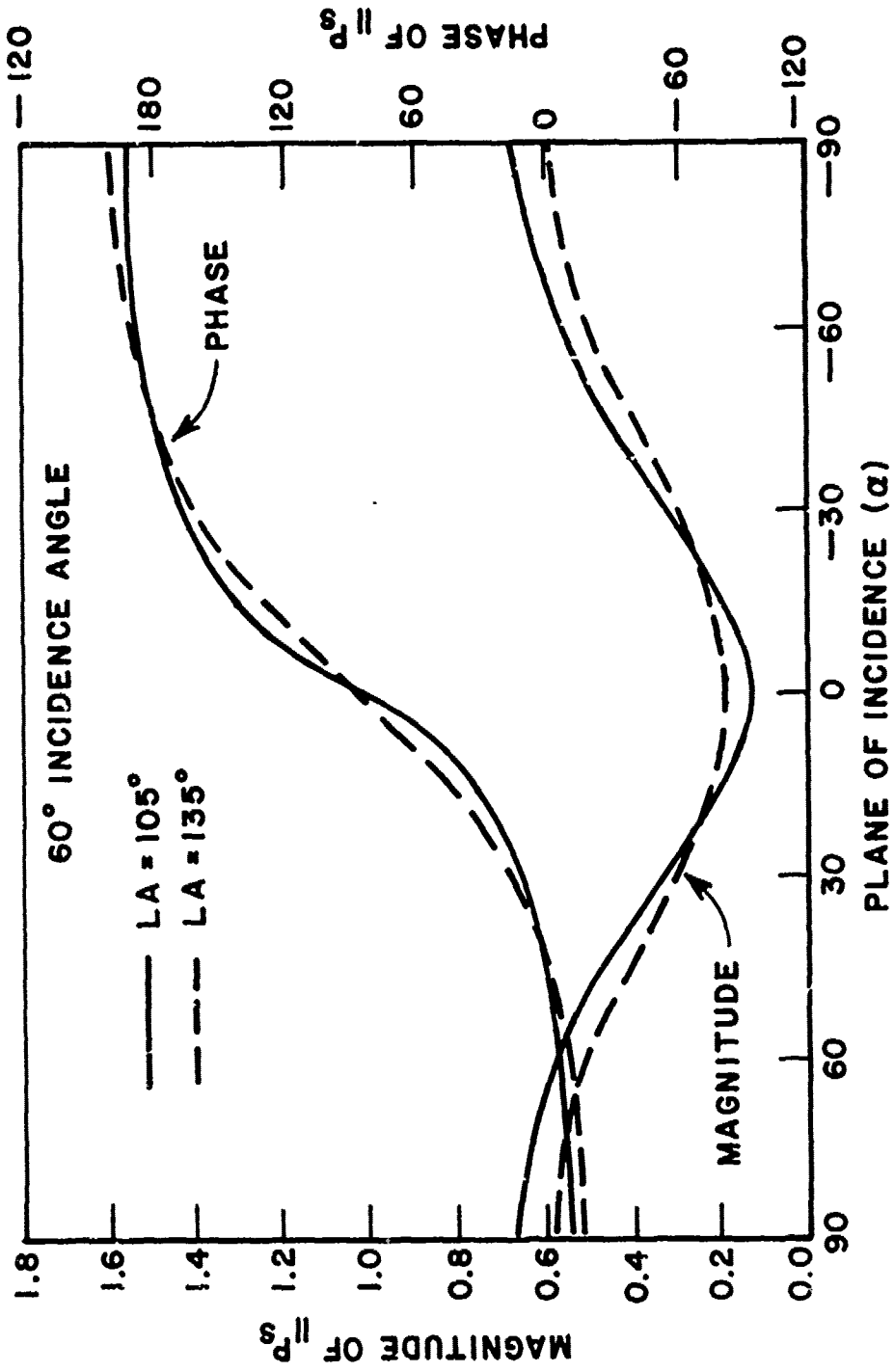


Figure 19. Parallel component of the pattern factor of the symmetric voltage mode for leg angles of 105° and 135°.

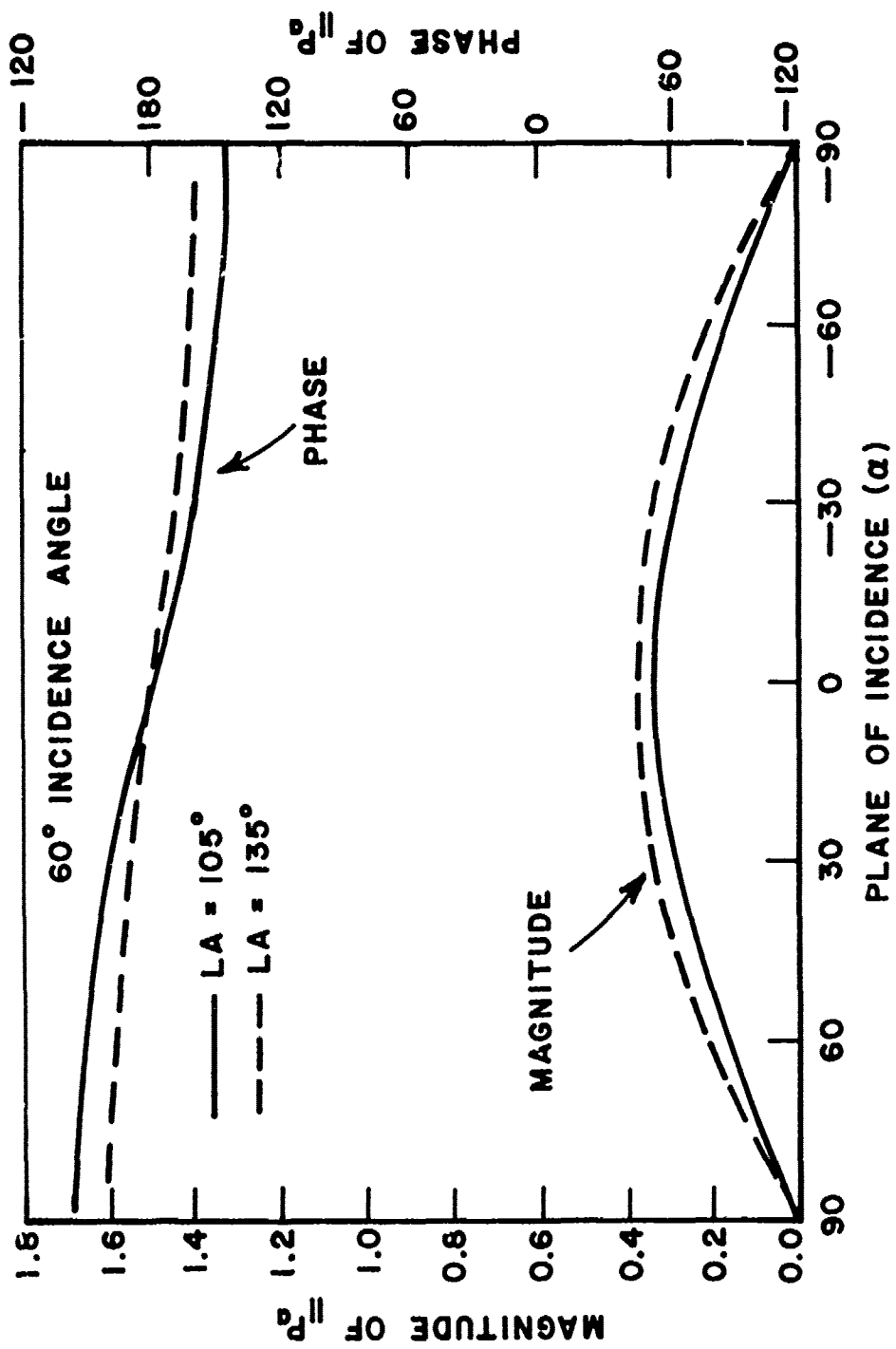


Figure 20. Parallel component of the pattern factor of the asymmetric voltage mode for leg angles of 105° and 135°.

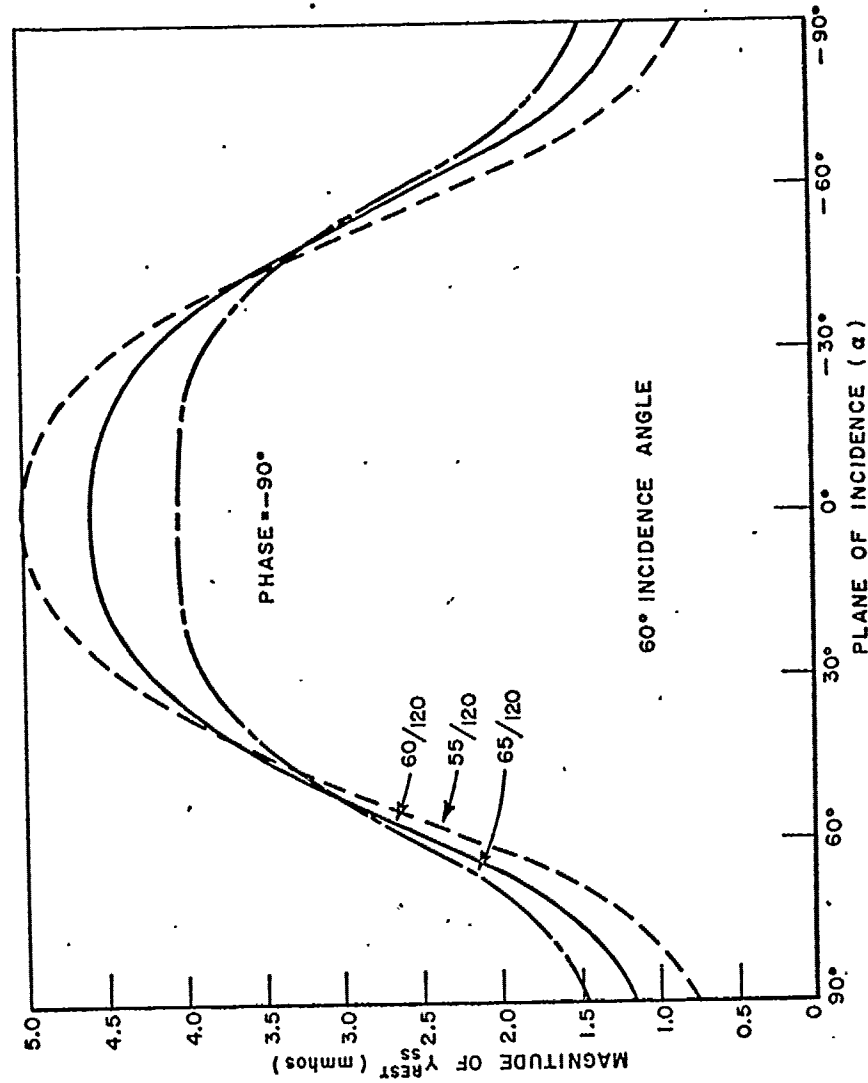


Figure 21. Magnitude of the admittance Y_{SS}^{rest} for various incidence directions at a frequency slightly below resonance. Depicted are the 60/120, 55/120, and 65/120 arrays. (The phase is -90°)

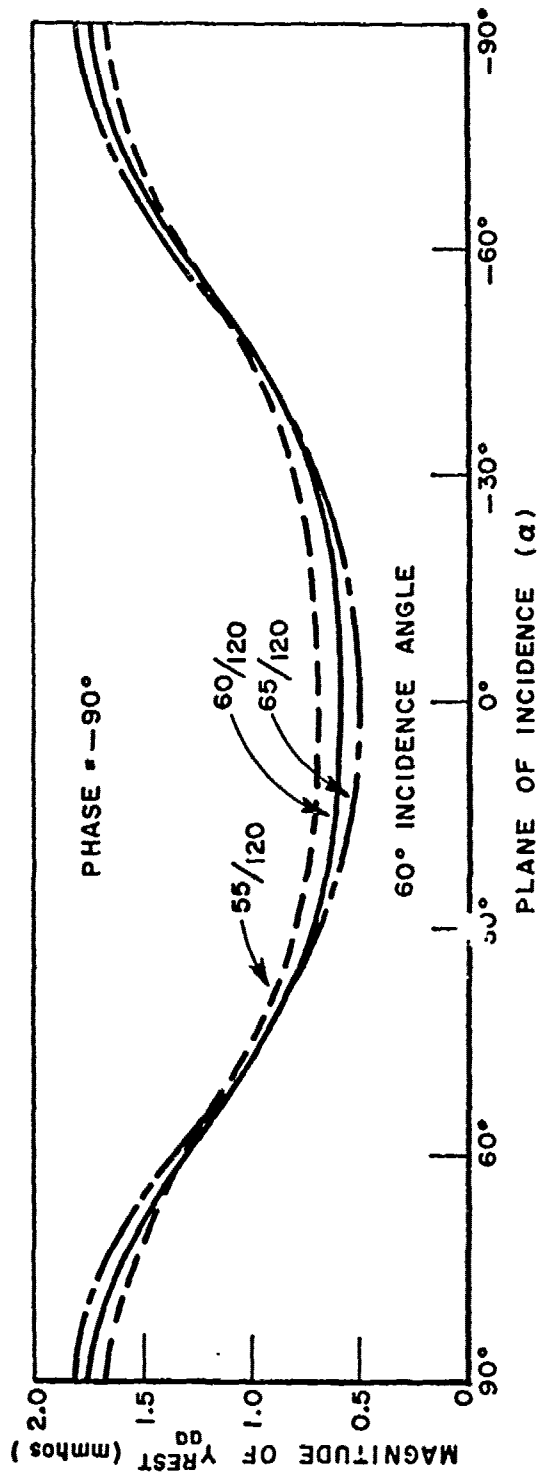


Figure 22. Magnitude of the admittance Y_{aa}^{rest} for various incidence directions at a frequency slightly below resonance. Depicted are the 60/120, 55/120 and 65/120 arrays. (The phase is -90°).

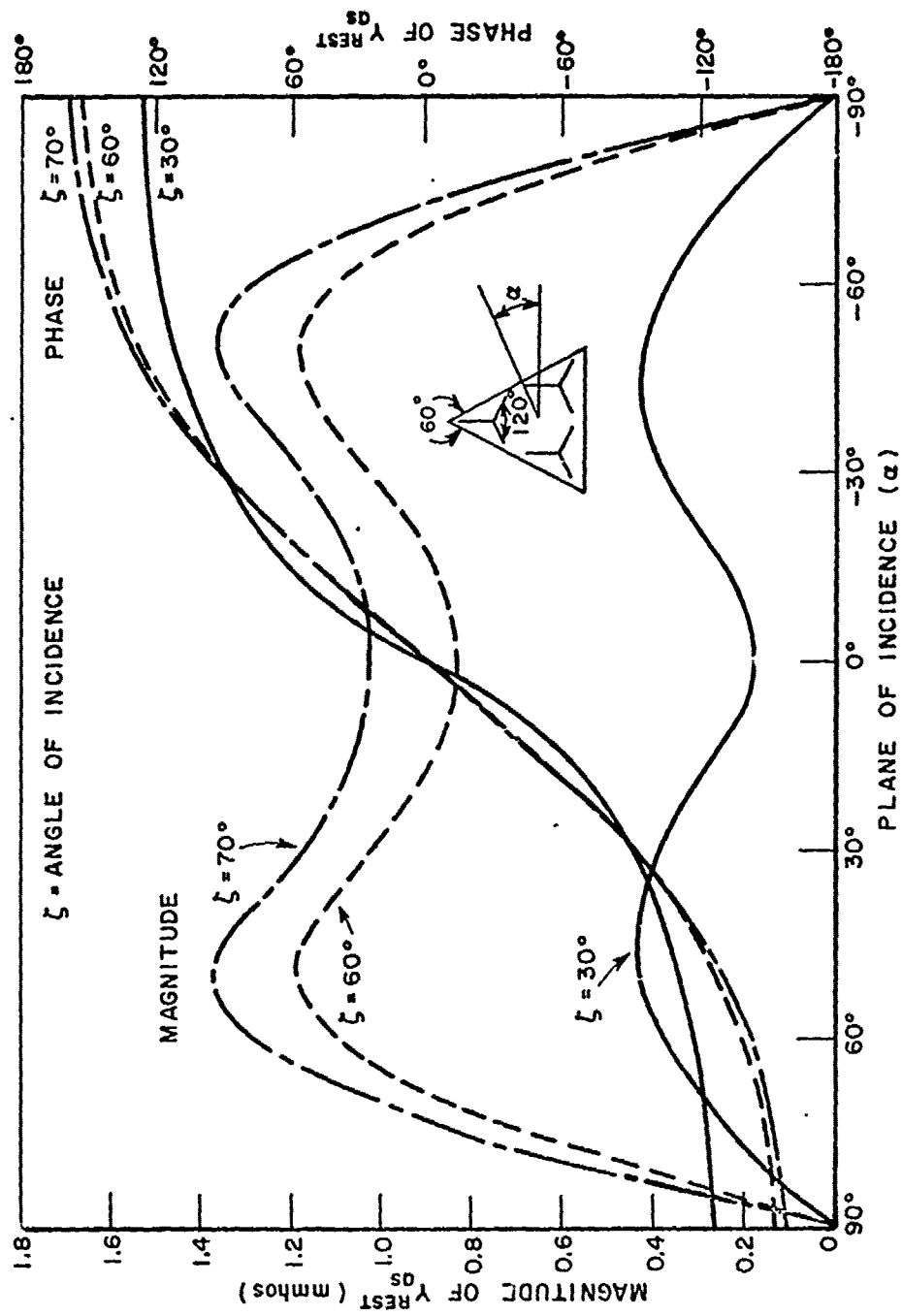


Figure 23. Magnitude (left scale) and phase (right scale) of the admittance y_{as}^{rest} for the 60/120 array. Frequency is slightly below resonance.

For the 60/120 array, optimum performance is obtained in the $\alpha=30^\circ$ and $\alpha=90^\circ$ planes (note that physically these planes look the same). While Y_{as}^{rest} is zero in the $\alpha=90^\circ$ plane, it is not in the $\alpha=30^\circ$ plane. The performance in both planes is the same, however. Equation (21) provides the answer to this quandary. At resonance (≈ 10.8 GHz), for the $\alpha=30^\circ$ and $\alpha=90^\circ$ planes, the parallel transmission is $-.02$ dB and the cross is negligible. For this to be true, Equation (21) must be satisfied in both cases. In the $\alpha=30^\circ$ case at 10.8 GHz, Equation (21) becomes; (see Appendix C)

$$a) \ .00302/\underline{-90} \stackrel{?}{=} \ .00329/\underline{-90} \quad (24a)$$

$$b) \ .00028/\underline{-90} \stackrel{?}{=} \ .000368/\underline{-90} \quad (24b)$$

As can be seen, the quantities are very close. The trend is such that, at resonance (≈ 10.75 GHz), both equalities hold and the parallel transmission is unity. In the $\alpha=90^\circ$ plane at 10.8 GHz; (from Appendix C)

$$a) \ 0.0 \stackrel{?}{=} \ 0.0 \frac{0.0}{.81/\underline{-165.3}} \quad (25a)$$

$$b) \ .0014/\underline{-90} \stackrel{?}{=} \ 0.0 \frac{.81/\underline{-165.3}}{0.0} \quad (25b)$$

The resonance mechanism illustrated above exemplifies the case where $Y_{as}^{rest} = 0$. It has been mentioned that, at one time, common belief was that Y_{as}^{rest} being zero was a necessary and sufficient condition for perfect performance for both polarizations. The reason for this assumption can be seen by observing Equations (21) and (22). Since the quantities

$$\frac{\perp P_s}{\perp P_a} \quad \text{and} \quad \frac{\parallel P_s}{\parallel P_a}$$

are quite independent, it seems logical that one way to make all equalities hold under the same conditions is to have both sides of the equations go to zero. However, the quantities shown in 25b) directly above show that, when Y_{as}^{rest} is zero in the $\alpha=90^\circ$ plane, $\perp P_s$ is also zero, yielding the indeterminate form 0/0. Also, by observing Figures 21 and 22, it can be seen that Y_{ss}^{rest} approaches

zero only in the $\alpha=90^\circ$ plane while Y_{aa}^{rest} approaches zero only in the $\alpha=0^\circ$ plane.

The $\alpha=90^\circ$ plane is a very special case in the study of arrays of generalized three legged elements, due to the symmetry of the voltage modes observed when scanning in this plane. The $\alpha=30^\circ$ plane is a better example of the resonance mechanism involved when optimum performance is achieved in a 60/120 array of generalized three legged elements.

In the $\alpha=0^\circ$ plane for the 60/120 array, at 10.8 GHz, Equation (21) becomes; (see Appendix C)

$$\text{a) } \underline{.0034/-90} \stackrel{?}{=} \underline{.0063/-90} \quad (26a)$$

$$\text{b) } \underline{.00014/-90} \stackrel{?}{=} \underline{.00013/-90} \quad (26b)$$

Both equalities do not hold, and, as seen in Figure 10, the performance is not optimum. There is no chance of achieving optimum performance in this plane with equi-length leg elements. However, since the phases of both sides of the equations are the same, modifications can be made to achieve optimum performance. The magnitude of Y_{SS}^{rest} may be changed with minimal effect on the other quantities by adjusting the length of the top leg. However, this improvement would be achieved at the price of the performance in the other planes.

At 10.8 GHz in the $\alpha=60^\circ$ plane, where the performance is the same as in the $\alpha=0^\circ$ plane, Equation (21) becomes: (Appendix C)

$$\text{a) } \underline{.0012/-90} \stackrel{?}{=} \underline{.0013/-70.9} \quad (27a)$$

$$\text{b) } \underline{.0009/-90} \stackrel{?}{=} \underline{.0011/-109.1} \quad (27b)$$

Here it appears that there is no way to obtain optimum performance since the phases are not even the same. However, using the insight from the $\alpha=0^\circ$ plane (physically the same) shows that optimum can be obtained by adjusting the length of the leg orthogonal to the $\alpha=60^\circ$ plane (the lower right hand leg), again at the expense of performance in the other planes. Apparently this would change the magnitude and phase of both sides of the equalities.

Using these examples, the truth of Munk's equations ((21) and (22)) may be seen. Now, the admittances for other grid/element combinations will be investigated. When the top grid angle is changed, the change will be such that the product $\Omega_x \Omega_z$ remains the same for all combinations (see Equation (19)).

Figure 24 shows Y_{as}^{rest} for a 55°/120° array slightly below resonance. Again, a seemingly shocking development arises. The phase for a 30° incidence angle attains 180° for the $\alpha=0$ plane instead of 0°. Figure 25, a polar plot of Y_{as} for an incidence angle of 30° for 60/120 and 55/120 arrays, clarifies this seeming discontinuity. Apparently at some grid angle between 55° and 60°, Y_{as} is identically zero for a 30° incidence angle in the $\alpha=0$ ° incidence plane. The same is true for higher incidence angles as the top grid angle is decreased more. However, it is now known that Y_{as}^{rest} being zero does not automatically indicate that optimum performance will be the result. For this case in particular, the performance, although good, is not quite optimized in the $\alpha=0$ ° plane as shown in Figure 12.

Equation (21) will now be applied to the $\alpha=60$ ° plane of the 55/120 array. At 10.8 gigahertz, which appears to be the resonant frequency of the parallel field from this incidence direction, the parallel transmission is -.14 dB and the cross is -18.5 dB, and Equation (21) becomes:

$$a) .00093/\underline{-90} \stackrel{?}{=} .0013/\underline{-57.4} \quad (28a)$$

$$b) .00092/\underline{-90} \stackrel{?}{=} .0011/\underline{-122.6} . \quad (28b)$$

The quantities differ in magnitude and phase, reaffirming the poor performance. If leg lengths could be adjusted to produce good performance in this ($\alpha=60$ °) plane, the performance in other planes would suffer.

Further inspecting Figure 24, it can be seen that the change in Y_{as}^{rest} with respect to the 60/120 array is very small except in the region $-45^\circ < \alpha < 45^\circ$, where the magnitude of Y_{as}^{rest} for the 55/120 array becomes smaller for all incidence angles.

Figure 26 shows Y_{as}^{rest} for a 65/120 array. The change in Y_{as}^{rest} again exists in the region $-45 < \alpha < 45$, but here in contrast to the 55/120 array, the magnitude for all incidence angles becomes larger.

From the preceding discussion, it becomes evident that the admittance curves of the 60/120 array (Figure 23) must be reproduced in order to obtain optimum performance for other array configurations. This will involve altering the magnitude in the $-45 < \alpha < 45$ region only. Figure 27 shows Y_{as}^{rest} for a 60/105 array. Notice that these curves look very similar to those for a 65/120 array, both resulting in a larger magnitude for the region $-45 < \alpha < 45$ than the 60/120 array. Thus, it appears that combining the 55/120 and the 60/105 array might produce the desired curves for Y_{as}^{rest} . Figure 28 shows Y_{as}^{rest} for the 55/105 array. Comparing these to the curves for the 60/120 array (Figure 23) show a great similarity, thus creating the "optimum" performance of the 55/105 array.

Figure 29 shows Y_{as}^{rest} for a 60/135 array. The curves here are similar to those in Figure 24 for the 55/120 array. Combining the 65/120 and 60/135 arrays into the 65/135 array produce the admittances shown in Figure 30. Again these admittances are similar to the admittances exhibited by the 60/120 array (Figure 23) and lead to the "optimum" performance of the 65/135 array.

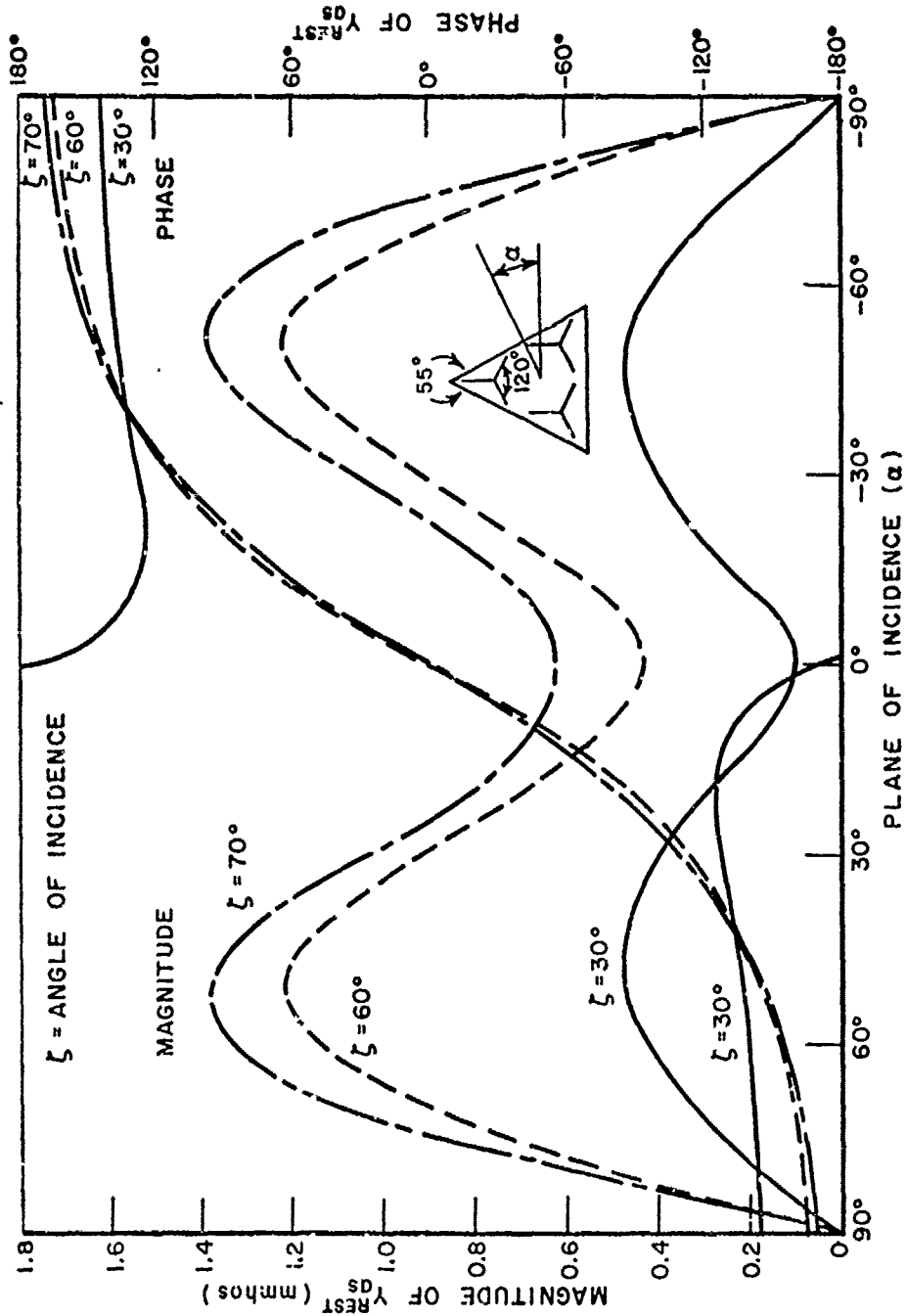


Figure 24. Magnitude (left scale) and phase (right scale) of the admittance Y_{DS}^{rest} for the 55/120 array. Frequency is slightly below resonance.

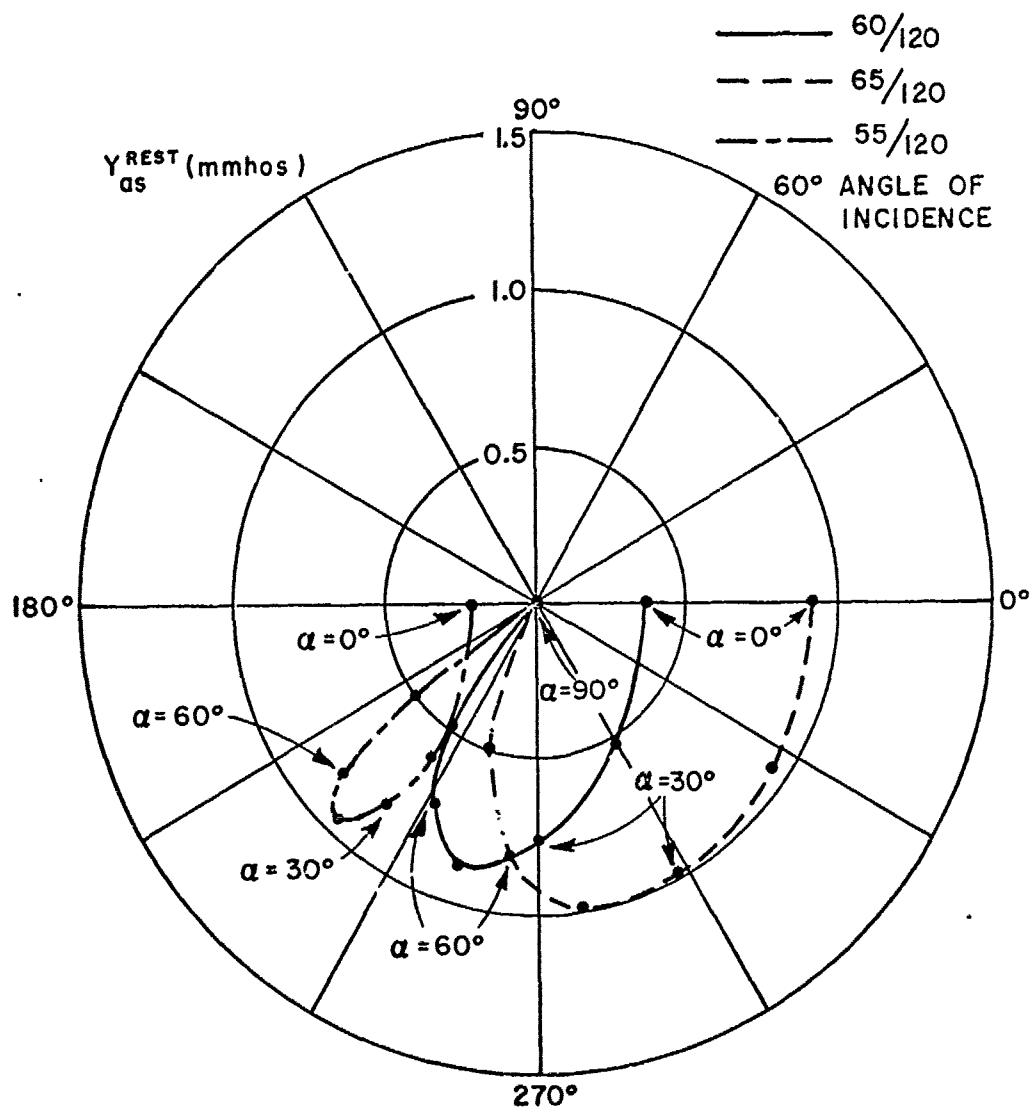


Figure 25. Polar plot of the admittance Y_{as}^{rest} for incidence angles of 30° for 65/120, 60/120, and 55/120 arrays. Frequency is slightly below resonance.

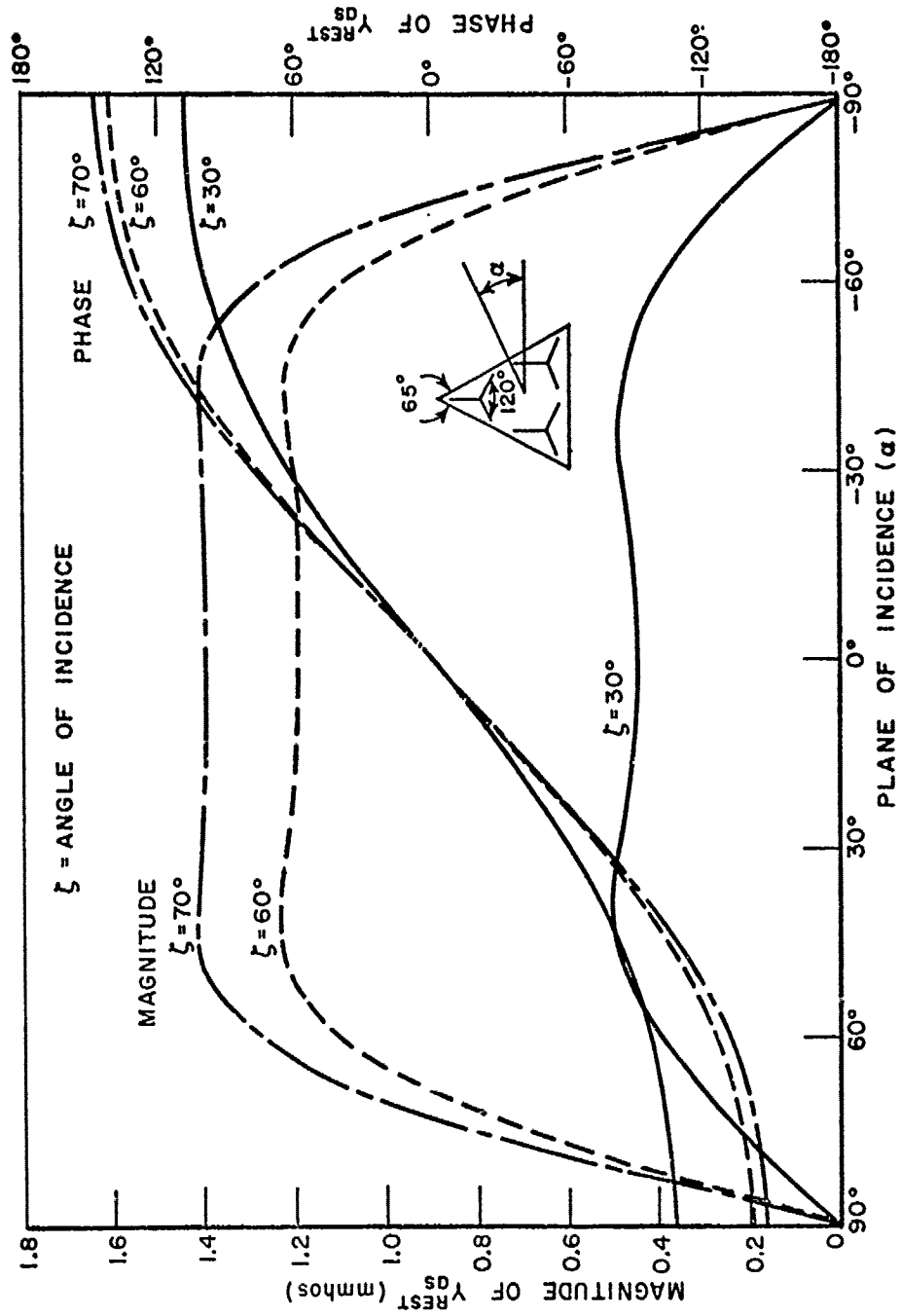


Figure 26. Magnitude (left scale) and phase (right scale) of the admittance. Y_{REST}^{gs} array. Frequency is slightly below resonance.

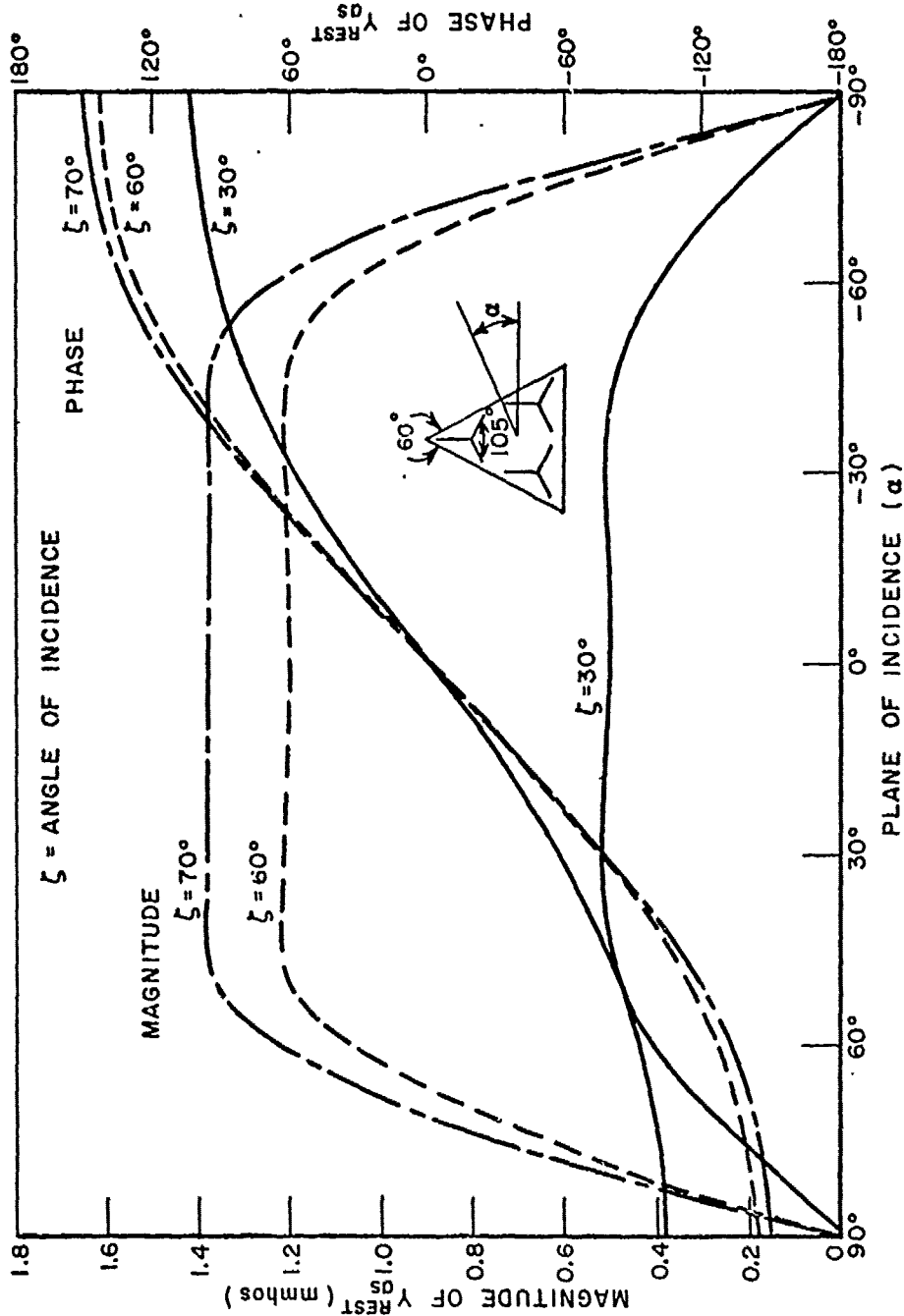


Figure 27. Magnitude (left scale) and phase (right scale) of the admittance Y_{as}^{rest} for the 60/105 array. Frequency is slightly below resonance.

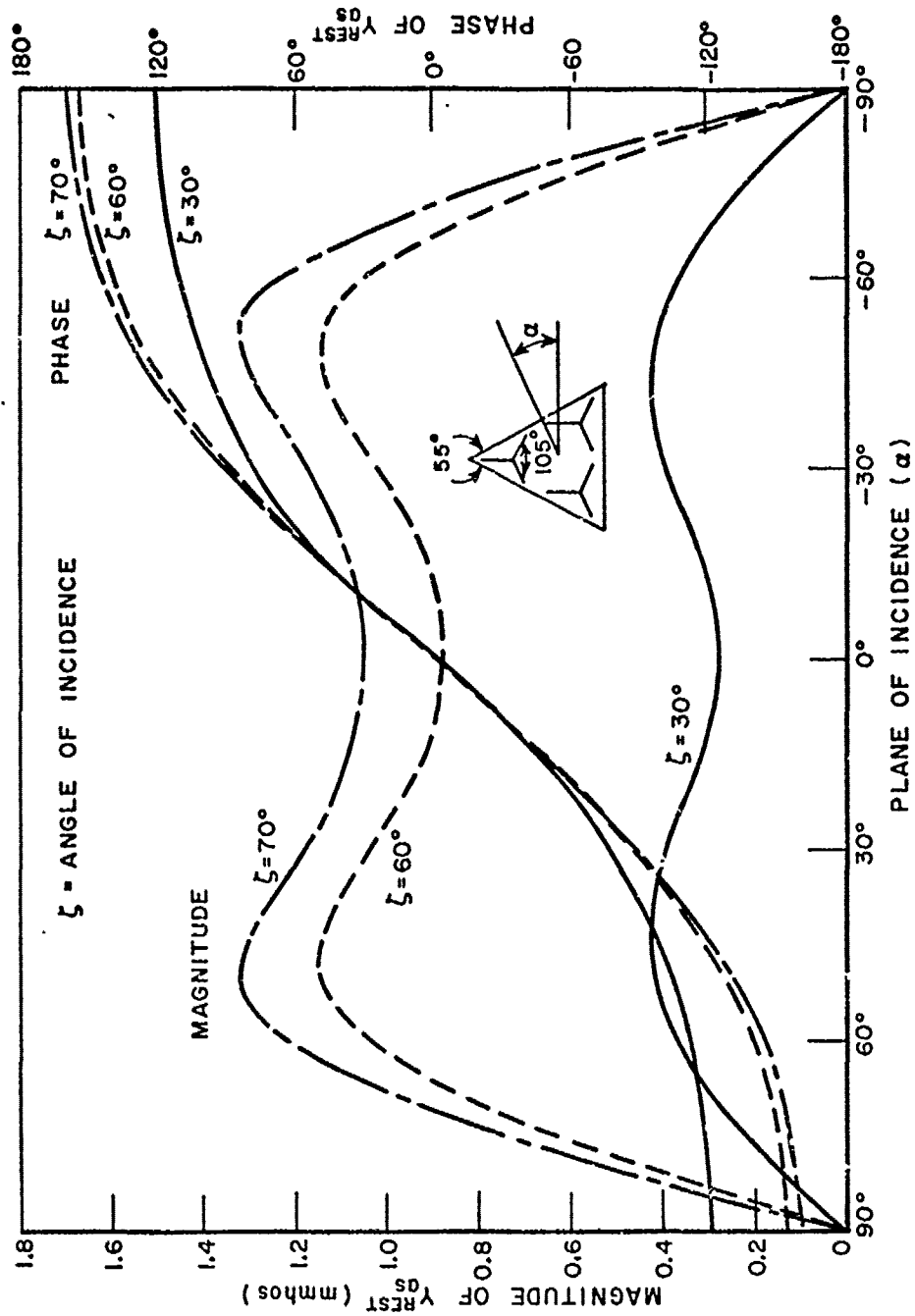


Figure 28. Magnitude (left scale) and phase (right scale) of the admittance Y_{AS}^{rest} for the 55/105 array. Frequency is slightly below resonance.

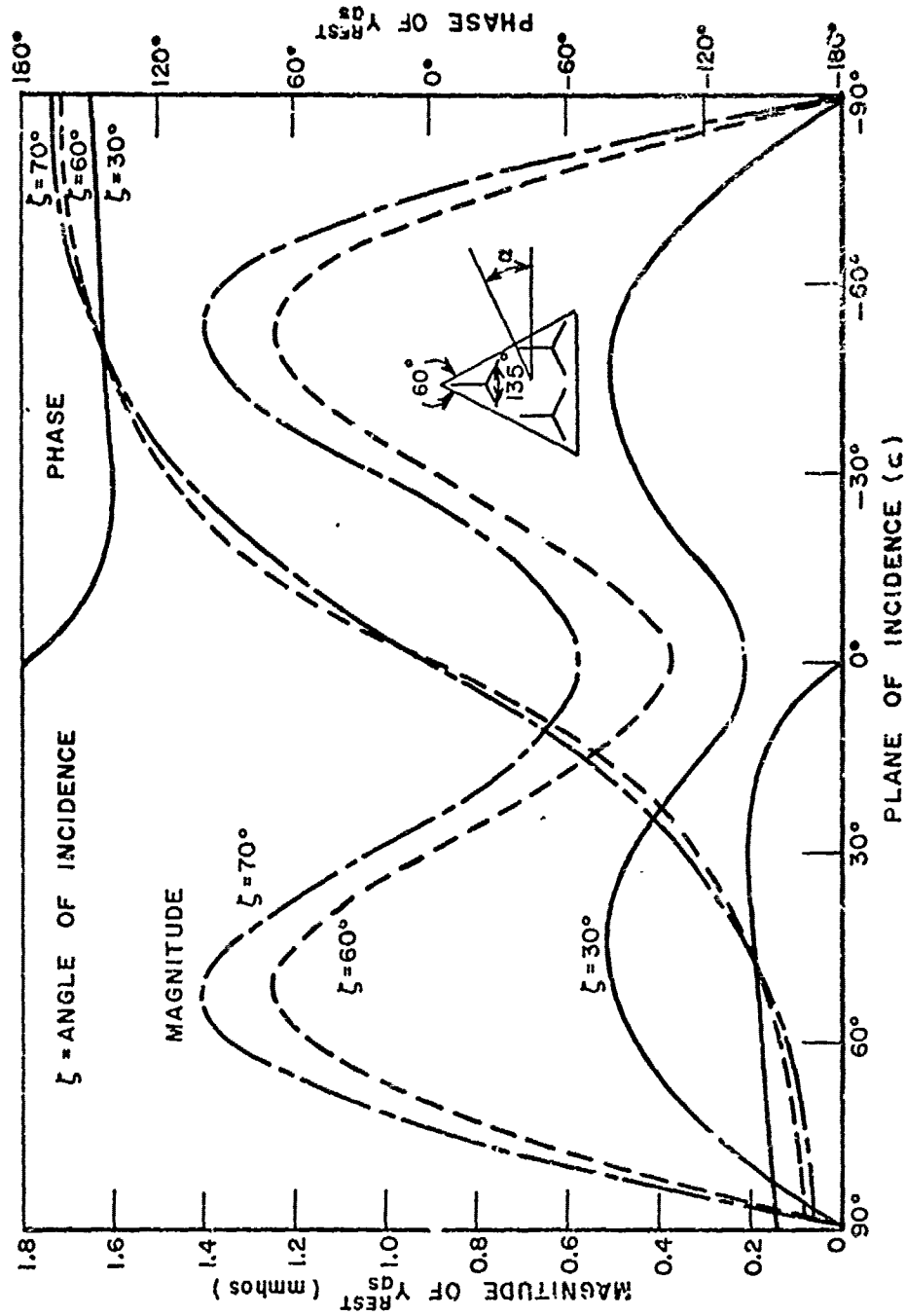


Figure 29. Magnitude (left scale) and phase (right scale) of the admittance Y_{rest} for the 60/135 array. Frequency is slightly below resonance.

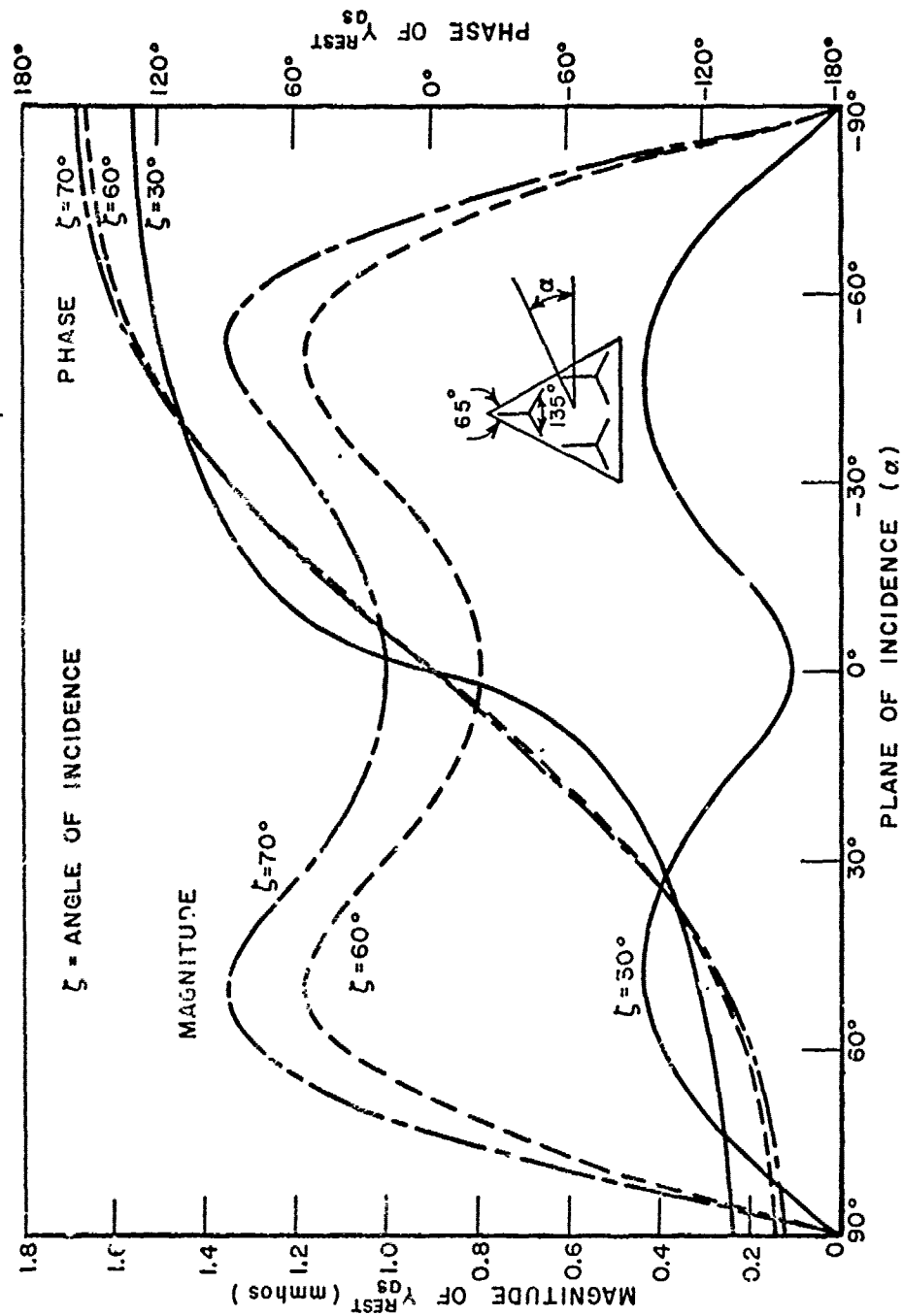


Figure 30. Magnitude (left scale) and phase (right scale) of the admittance Y_{AS}^{rest} for the 65/135 arrays. Frequency is slightly below resonance.

SECTION IV CONCLUSIONS

The introduction of arbitrary grid structure to the Plane Wave Expansion Method of calculating performance of periodic arrays requires a simple modification to the rectangular grid case. This modification has been successfully integrated into computer programs which could previously only calculate the performance of arrays with rectangular grids.

The results of the investigation in this report may also be used to calculate the onset of grating lobes in arrays with arbitrary grid structure.

To date, the prime use of the ability to calculate the performance of arrays with arbitrary grid structure has been to investigate the performance of arrays of generalized three legged elements. Arrays of this type will find wide use in the development of metallic radomes. It has been found that various grid geometries are required to "fit" a radome with an array of slots. By using the method developed in this report, a family of grid/element geometries has been found which yields optimum performance. The grid/element combinations are centered about an array with an equilateral triangular grid and 120° between the legs of the elements. The equilateral triangular grid results in a basic grid angle of 60° . If the grid angle must be changed by a particular amount in order to "fit" the radome surface, the angle between the legs of each element must be changed by approximately three times that amount.

In the course of obtaining the optimum grid/element combinations, it was found that the key to the performance of an array of generalized three legged elements is the mutual admittance between voltage modes which exist on the elements. Munk has predicted the relationship between the performance of arrays of generalized three legged elements and the mutual admittances mentioned above [19]. The work performed in this report shows the validity of Munk's predicted relationship for arrays in free space.

Although this report deals strictly with arrays in free space, the results have been applied to arrays imbedded in dielectric. It has been found that the presence of dielectric can actually enhance the performance of an array. A grid/element combination which has been optimized in free space also performs well when imbedded in dielectric. This fact is an important observation, as radome applications require that the array be imbedded in dielectric.

APPENDIX A
GRATING LOBES IN ARRAYS HAVING A SKEWED GRID

In the text, it was mentioned that the only difference between impedances of dipole arrays having rectangular and arbitrary grid structure (assuming no grating lobes) is in the real part. As it stands, this statement violates the property of analytic functions which state that the real and imaginary part of an analytic function are not independent. From this property, it follows that, if the real part of the impedance changes, the imaginary part must also change for the two cases. The answer to this apparent flow is explained by the following development concerning the onset of grating lobes. This development shows that grating lobes appear at different frequencies for the two cases, which explains the difference in the imaginary parts of the impedance functions.

$$1 - r(k,n)_x^2 - r(k,n)_z^2 = 0 \quad (A1)$$

$$k, n \neq 0 .$$

Realizing that grating lobes first occur for grazing incidence set

$$r(i)_x^2 + r(i)_z^2 = 1 \quad (A2)$$

Substituting Equation (A2) and Equation (19) from the text into (A1);

$$\lambda = - \frac{2 \left(k \left(\frac{r(i)_x}{D_x} \right) + n \left(\frac{r(i)_z}{D_z} - \frac{r(i)_x}{D_x} \frac{\Delta z}{D_z} \right) \right)}{\frac{k^2}{D_x^2} - 2kn \frac{\Delta z}{D_x^2 D_z} + n^2 \left(\frac{1}{D_z^2} + \frac{\Delta z^2}{D_x^2 D_z^2} \right)} \quad (A3)$$

At this point two grating lobe occurrences will be investigated:

$$\begin{aligned} k=-1 \quad n=0 \\ \lambda = \frac{2 \frac{r(i)_x}{D_x}}{\frac{1}{D_x^2}} \end{aligned}$$

$$= 2r(i)_x D_x$$

$$\begin{aligned} n=-1 \quad k=0 \\ \lambda = \frac{2 \left(\frac{r(i)_z}{D_z} - \frac{r(i)_x}{D_x} \frac{\Delta z}{D_z} \right)}{\left(\frac{1}{D_z^2} + \frac{\Delta z^2}{D_x^2 D_z^2} \right)} \end{aligned}$$

$$= 2D_x D_z \left(\frac{r(i)_z D_x - r(i)_x \Delta z}{D_x^2 + \Delta z^2} \right)$$

Thus, it can be seen that, with the addition of Δz (skewing the grid), the grating lobe associated with the $n=-1, k=0$ term occurs at a different frequency (wavelength) than with a rectangular grid ($\Delta z=0$). For example, assume grazing incidence such that $r(i)_x = r(i)_z = \sqrt{2}/2$, $D_x=D_z=2$ cm., and $\Delta z = D_z/2 = 1$ cm.

$$\lambda_{gl} = 8 \left(\frac{\sqrt{2} \cdot \sqrt{2}}{4 + 1} \right) = \frac{8}{5} \sqrt{2} \text{ cm}$$

or 26.52 GHz.

However, for a rectangular grid ($\Delta z=0$),

$$\lambda_{gl} = 8 \left(\frac{\sqrt{2}}{4} \right) = 2 \sqrt{2} \text{ cm}$$

or 10.61 GHz.

It can be seen that making the grid arbitrary delays the onset of this particular grating lobe. However, in both arrays, other grating lobes will occur at other values of k and n for other incidence planes. When all are considered, the skewed grid array grating lobes will not be delayed as much as this particular one. The point being made here is that grating lobes do occur at different frequencies for a skewed grid as opposed to a rectangular grid.

APPENDIX B
ARRAY GRID ANGLE RELATIONSHIPS

The purpose of this appendix is to establish the relationship between the two grid angles of an array (top and side). Figure B1 depicts the grid structure of an array. The points represent element centers. Choosing the angles A and B on the figure:

$$2A = \text{TGA (Top Grid Angle)}$$

$$2B = \text{SGA (Side Grid Angle)}.$$

By geometry:

$$\tan A = \frac{D_x}{3(D_x \tan B)} = \frac{1}{3 \tan B}$$

With this relationship, the following table may be obtained:

TGA	SGA
50	71.12
55	65.26
60	60.00
65	55.24
70	50.92

This result can be of great utility when fitting an array to a radome. For example, some regions of a particular radome may require a basic grid angle of 55°, and others an angle of 65°. Both angles may be realized with arrays having identical elements. When fitting any radome with a periodic surface however, care must be exercised in order to minimize the number of elements lost on the boundaries of regions having different grid angles.

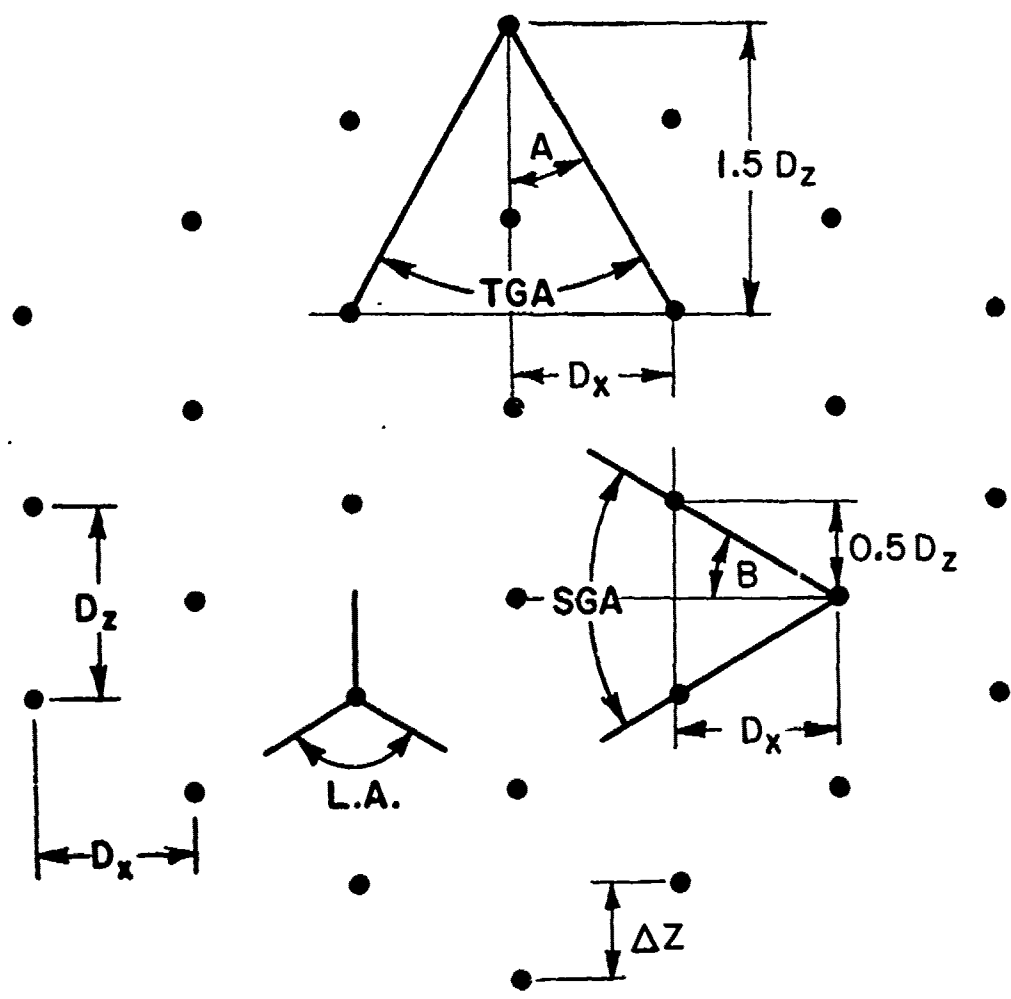


Figure B1. General skewed grid structure showing the relationship between the top and side grid angles.

APPENDIX C
SAMPLE CALCULATIONS OF ADMITTANCE RELATIONSHIPS

This appendix supports the admittance relationships for various planes of incidence cited in the analysis portion of the third chapter.

I. 60/120 array

A. $\alpha = 30$

$$Y_{ss} = .00302/\underline{-90}$$

$$Y_{sa} = .0011/\underline{-90}$$

$$Y_{aa} = .00028/\underline{-90}$$

$$Y_{as} = .0011/\underline{-90}$$

$$\perp P_a = .405/\underline{165.3}$$

$$\perp P_s = 1.21/\underline{165.3}$$

$$24a) \ .00302/\underline{-90} \stackrel{?}{=} .0011/\underline{-90}$$

$$\frac{1.21/\underline{165.3}}{.405/\underline{165.3}}$$

$$= .00329/\underline{-90}$$

$$24b) \ .00028/\underline{-90} \stackrel{?}{=} .0011/\underline{-90}$$

$$\frac{.405/\underline{165.3}}{1.21/\underline{165.3}}$$

$$= .000368/\underline{-90}$$

B. $\alpha = 90^\circ$

$$Y_{ss} = 0.0$$

$$Y_{sa} = 0.0$$

$$Y_{aa} = .0014/\underline{-90}$$

$$Y_{as} = 0.0$$

$$\perp P_a = .81/\underline{-165.3}$$

$$\perp P_s = 0.0$$

$$25a) 0.0 \stackrel{?}{=} 0.0 \frac{0.0}{.81/-165.3}$$

$$25b) .0014/-90 \stackrel{?}{=} 0.0 \frac{.81/-165.3}{0.0}$$

C. $\alpha = 0^\circ$

$$Y_{ss} = .0034/-90$$

$$Y_{sa} = .00091/180$$

$$Y_{aa} = .00014/-90$$

$$Y_{as} = .00091/0$$

$$\perp P_a = .195/90$$

$$\perp P_s = 1.358/180$$

$$26a) .0034/-90 \stackrel{?}{=} .00091/-180$$

$$\frac{1.358/180}{.195/90}$$

$$= .0063/-90$$

$$26b) .00014/-90 \stackrel{?}{=} .00091/0$$

$$\frac{.195/180}{1.358/180}$$

$$= .00013/-90$$

D. $\alpha = 60^\circ$

$$Y_{ss} = .0012/-90$$

$$Y_{sa} = .0012/-39.3$$

$$Y_{aa} = .0009/-90$$

$$Y_{as} = .0012/-140.7$$

$$\perp P_a = .686/-171.8$$

$$\perp P_s = .739/156.6$$

$$\begin{aligned}
 27a) \quad & \frac{.0012/-90}{=} \stackrel{?}{=} \frac{.0012/-39.3}{=} \frac{.739/156.6}{.686/-171.8} \\
 & = \frac{.0013/-70.9}{=} \\
 27b) \quad & \frac{.0009/-90}{=} \stackrel{?}{=} \frac{.0012/-140.7}{=} \frac{.686/-171.8}{.739/156.6} \\
 & = \frac{.0011/-109.1}{=}
 \end{aligned}$$

II. 55/120 array

$$\alpha = 60^\circ$$

$$\begin{aligned}
 Y_{ss} &= \frac{.00093/-90}{} & Y_{sa} &= \frac{.0012/-25.8}{} \\
 Y_{aa} &= \frac{.00092/-90}{} & Y_{as} &= \frac{.0012/-154.2}{} \\
 \perp P_a &= \frac{.686/-171.8}{} & \perp P_s &= \frac{.739/156.6}{}
 \end{aligned}$$

$$\begin{aligned}
 28a) \quad & \frac{.00093/-90}{=} \stackrel{?}{=} \frac{.0012/-25.8}{=} \frac{.739/156.6}{.686/-171.8} \\
 & = \frac{.0013/-57.4}{=}
 \end{aligned}$$

$$\begin{aligned}
 28b) \quad & \frac{.00092/-90}{=} \stackrel{?}{=} \frac{.0012/-154.2}{=} \frac{.686/-171.8}{.739/156.6} \\
 & = \frac{.0011/-122.6}{=}
 \end{aligned}$$

REFERENCES

- [1] Munk, B. A., Pelton, E. L., Larson, C. J., and Kornbau, T. W., "RCS Reduction Studies," Report 3622-10, November 1976, The Ohio State University ElectroScience Laboratory, Department of Electrical Engineering; prepared under Contract F33615-73-C-1173 for Air Force Avionics Laboratory, Wright-Patterson Air Force Base, Ohio, p. 177. (AFAL-TR-76-214)
- [2] Pelton, E. L., "Scattering Properties of Periodic Arrays Consisting of Resonant Multi-Mode Elements," Report 3622-3, March 1975, The Ohio State University ElectroScience Laboratory, Department of Electrical Engineering; prepared under Contract F33615-73-C-1173 for Air Force Avionics Laboratory, Wright-Patterson Air Force Base, Ohio. (AFAL-TR-75-98) (AD/A 016950)
- [3] Munk, B. A., Burrell, G. A., and Kornbau, T. W., "Plane Wave Expansion for Arrays of Arbitrary Oriented Piecewise Linear Elements," Report 4346-1, (in preparation), The Ohio State University ElectroScience Laboratory, Department of Electrical Engineering; prepared under Contract F33615-76-C-1024 for Air Force Avionics Laboratory, Wright-Patterson Air Force Base, Ohio.
- [4] Papoulis, A., The Fourier Integral and its Applications, McGraw-Hill, 1962, p. 47.
- [5] Munk, B. A. and Kornbau, T. W., "Generalized Three Legged Elements in Stratified Dielectric Media," Report 4346-6, (in preparation), The Ohio State University ElectroScience Laboratory, Department of Electrical Engineering; prepared under Contract F33615-76-C-1024 for Air Force Avionics Laboratory, Wright-Patterson Air Force Base, Ohio.
- [6] Papoulis, A., The Fourier Integral and its Applications, op. cit., p. 47.
- [7] Ibid., p. 15.
- [8] Bateman, H., Table of Integral Transforms, Vol. 1, McGraw-Hill, 1954.
- [9] Ibid.
- [10] Munk, B. A. Burrell, G. A., and Kornbau, T. W., op. cit.
- [11] Pelton, E. L., "Scattering Properties of Periodic Arrays Consisting of Resonant Multi-Mode Elements," op. cit.

- [12] Munk, B. A. and Kornbau, T. W., "Generalized Three Legged Elements in Stratified Dielectric Media," op. cit.
- [13] Ibid.
- [14] Pelton, E.L., "A Streamlined Metallic Radome with High Transmission Performance," Report 2989-11, March 1973, The Ohio State University ElectroScience Laboratory, Department of Electrical Engineering; prepared under Contract F33615-70-C-1439 for Air Force Avionics Laboratory, Wright-Patterson Air Force Base, Ohio. (AFAL-TR-73-100) (AD 909360L)
- [15] Ibid.
- [16] Munk, B. A. and Kornbau, T. W., "Generalized Three Legged Elements in Stratified Dielectric Media," op. cit.
- [17] Munk, B. A., Pelton, E. L., Larson, C. J., and Kornbau, T.W., "RCS Reduction Studies," op. cit.
- [18] Munk, B. A. and Kornbau, T.W., "Generalized Three Legged Elements in Stratified Dielectric Media," op. cit.
- [19] Ibid.